Planetary and Space Science 58 (2010) 327–350

Contents lists available at ScienceDirect

Planetary and Space Science

journal homepage: www.elsevier.com/locate/pss

Saturn's magnetospheric interaction with Titan as defined by Cassini encounters T9 and T18: New results

E.C. Sittler Jr.[a,*], R.E. Hartle[a], R.E. Johnson[b], J.F. Cooper[a], A.S. Lipatov[a,c], C. Bertucci[d], A.J. Coates[e], K. Szego[f], M. Shappirio[a], D.G. Simpson[a], J.-E. Wahlund[g]

[a] NASA Goddard Space Flight Center, Greenbelt, MD, USA
[b] University of Virginia, Charlottesville, VA, USA
[c] University of Maryland in Baltimore, Maryland, USA
[d] Institute for Astronomy and Space Physics, Buenos Aires, Argentina
[e] Mullard Space Science Laboratory, University College London, Dorking, UK
[f] KFKI Research Institute for Particle and Nuclear Physics, Budapest, Hungary
[g] Swedish Institute of Space Physics, Upsalla, Sweden

ARTICLE INFO

Article history:
Received 7 July 2009
Received in revised form
12 September 2009
Accepted 19 September 2009
Available online 24 October 2009

Keywords:
Titan
Saturn's magnetosphere
Magnetodisc
Plasma
Magnetic fields
Ion composition

ABSTRACT

We present new results of Cassini's T9 flyby with complementary observations from T18. Based on Cassini plasma spectrometer (CAPS) and Cassini magnetometer (MAG), compositional evidence shows the upstream flow for both T9 and T18 appears composed of light ions (H^+ and H_2^+), with external pressures ~30 times lower than that for the earlier TA flyby where heavy ions dominated the magnetospheric plasma. When describing the plasma heating and sputtering of Titan's atmosphere, T9 and T18 can be considered interactions of low magnetospheric energy input. On the other hand, T5, when heavy ion fluxes are observed to be higher than typical (i.e., TA), represents the limiting case of high magnetospheric energy input to Titan's upper atmosphere. Anisotropy estimates of the upstream flow are $1 < T_\perp/T_\parallel < 3$ and the flow is perpendicular to **B**, indicative of local picked up ions from Titan's H and H_2 coronae extending to Titan's Hill sphere radius. Beyond this distance the corona forms a neutral torus that surrounds Saturn. The T9 flyby unexpectedly resulted in observation of two "wake" crossings referred to as Events 1 and 2. Event 2 was evidently caused by draped magnetosphere field lines, which are scavenging pickup ions from Titan's induced magnetopause boundary with outward flux $\sim 2 \times 10^6$ ions/cm^2/s. The composition of this out flow is dominated by H_2^+ and H^+ ions. Ionospheric flow away from Titan with ion flux $\sim 7 \times 10^6$ ion/cm^2/s is observed for Event 1. In between Events 1 and 2 are high energy field aligned flows of magnetosphere protons that may have been accelerated by the convective electric field across Titan's topside ionosphere. T18 observations are much closer to Titan than T9, allowing one to probe this type of interaction down to altitudes ~950 km. Comparisons with previously reported hybrid simulations are made.

Published by Elsevier Ltd.

1. Introduction

We present new Cassini plasma and magnetic field results from the T9 encounter with Titan with complementary measurements from the T18 encounter. The Cassini mission is composed of many Titan flybys seeking to understand dynamics of magnetospheric interactions with upper atmosphere of Titan. The T9–T18 pair of flybys, as discussed below, are of special interest because of similar local times for Titan and, hence, similar solar illumination conditions. In addition, the magnetosphere is locally in magnetodisk configuration, the plasma density is low and the upstream ion compositions are similar.

Numerous papers have been published on the T9 flyby giving preliminary results (Szego et al., 2007; Coates et al., 2007a, b; Bertucci et al., 2007; Modolo et al., 2007a; Wei et al., 2007). Numerical models of the encounter were also presented (Modolo et al., 2007b) using an ion composition for the upstream flow similar to that for Voyager 1, which contained a light and a heavy ion component (Neubauer et al., 1984; Hartle et al., 2006a, b). Here we show that at local time ~0300 h the composition for the upstream plasma for T9 contained only light ions, a result of the magnetodisk structure for local times dusk to midnight to dawn as originally shown by Arridge et al. (2007, 2008a,b). Comprehensive electron parameters for Saturn's magnetotail, including local times similar to that for T9, have recently been published by Arridge et al. (2009). We present Cassini plasma spectrometer (CAPS) observations showing that Titan was below the current sheet of the magnetosphere at the time of T9 (see also Bertucci

* Corresponding author. Tel.: +1 301 286 9215; fax: +1 301 286 1433.
E-mail address: edward.c.sittler@nasa.gov (E.C. Sittler Jr.).

0032-0633/$ - see front matter Published by Elsevier Ltd.
doi:10.1016/j.pss.2009.09.017

et al., 2009) and that the current sheet was probably moving upward. Sittler et al. (2009a) argued that heavy ions are expected to be confined within ~2° of the current sheet, while at higher magnetic latitudes, on so-called lobe field lines, the ion densities are low, $n_P \leq 0.1$ ions/cm^3, and primarily composed of protons and H_2^+ ions (see Maurice et al., 1997).

Under the upstream conditions for T9, the combined ram pressure and plasma pressure are ~30 times lower than that for both TA (Hartle et al., 2006a, b; Backes et al., 2005; Neubauer et al., 2006; Modolo and Chanteur, 2008) and Voyager 1 (Hartle et al., 1982; Gurnett et al., 1982; Neubauer et al., 1984; Sittler et al., 2005). With reduced external plasma pressure the induced magnetopause boundary, around which the magnetospheric plasma is diverted, is expected to move radially outward from the topside ionosphere. This effect is somewhat countered by Saturn's magnetospheric field having a greater intensity below the current sheet (i.e., Harris current sheet model, see Arridge et al., 2007), when it is in a magnetodisk configuration (Bertucci et al., 2009). The stronger magnetic field helps shield Titan's upper atmosphere and exosphere from magnetospheric protons and electrons, which have smaller gyro-radii than heavy ions. This reduced access to Titan's upper atmosphere translates to less energy input so that EUV photons dominate the energy input at all relevant altitudes.

The induced magnetopause, the outer boundary of the interaction region, defines a cavity within which the convection electric field nearly vanishes. Therefore, magnetospheric electrons have reduced access to Titan's thermosphere/exosphere, so that electron impact ionization of CH_4 and N_2 are less important. This accounts for the lack of detection of methane and molecular nitrogen pickup ions during the T9 encounter (Szego et al., 2007). But, as shown later, mass 16 ions were briefly detected during Event 2. If EUV photons dominate the ionization within the cavity, this might explain why H_2^+ ions, rather than H^+, dominate Event 2. That is ionizing EUV photons predominantly produce H_2^+ (non-dissociative ionization $H_2 + h\nu \rightarrow H_2^+ + e$; Huebner and Giguere, 1980) rather than H^+. If dissociative ionization by electron impact had been dominant, the primary pickup ion would have been H^+ (Rapp and Englander-Golden, 1965). Low-energy charge exchange reactions between H^+ and H_2 will not dissociate H_2 but can be shown to be less likely than electron impact ionization (see Sittler et al., 2005).

The T9 flyby occurred relatively far from Titan, so the much closer T18 flyby was used for direct measurement of the induced magnetopause. Similarly to T9, the T18 upstream flow was composed only of protons and H_2^+, had a low density < 0.1 el/cm^3, and occurred at similar local time ~0300 h with the magnetospheric field in a magnetodisk configuration. T9 and T18 can be used to constrain hybrid simulations [Lipatov et al., 2009] of the interaction with H_2 exobase density and ionospheric wind as free parameters. One of the discoveries for T9 was observance of two crossings (Szego et al., 2007; Coates et al., 2007a, b). The observations reported here do not require a split tail as modeled by Modolo et al. (2007b). Rather, Event 1 is like the classical induced magnetotail as observed during the TA flyby (Hartle et al., 2006a, b) and Event 2 is more likely due to magnetic field lines draped around Titan, which "direct" the observed H_2^+ pickup ions formed upstream in the extended H_2 exosphere. Event 2 can also be explained as a scavenging mechanism or two-stream instability as discussed in Dobe et al. (2007).

2. Flyby geometries for T9 and T18

The T9 encounter geometry is shown in Fig. 1 as previously reported by Szego et al. (2007). Fig. 2 gives the encounter geometry for T18 with a similar format but also including

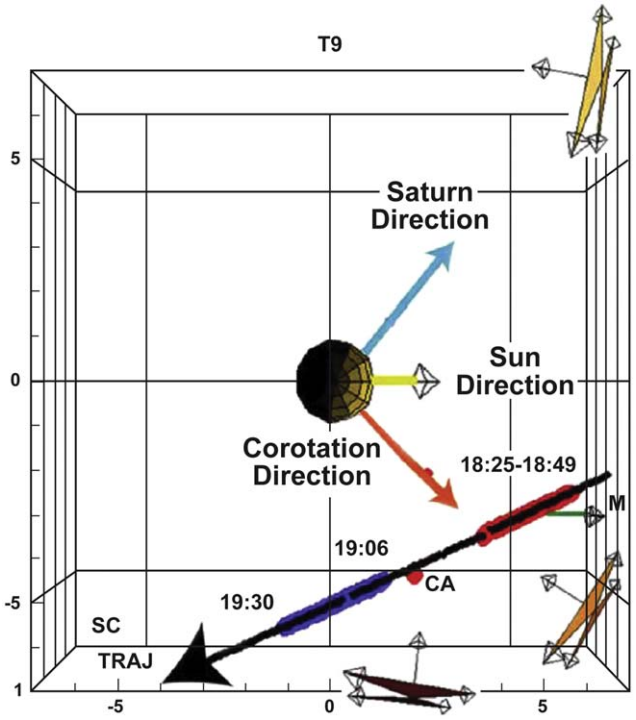

Fig. 1. Cassini T9 encounter trajectory plot from Szego et al. (2007) showing the geometry of the encounter. The Saturn equatorial reference frame (SSQ) is used, with x–y plane in Saturn's equatorial plane and z aligned with Saturn's spin axis. The x-axis is the abscissa and the y-axis the ordinate with z projected outward with 3D projection used. The solar direction is in the z–x plane where it is 19° below the x-axis. It shows the position intervals of Event 1 (red band) and Event 2 (blue band), respectively before and after closest approach (CA) along the spacecraft track. Also indicated are the solar illumination of Titan's upper atmosphere for the approach trajectory period, the corotation direction and the velocity vector of the spacecraft then moving away from Saturn. Here, the upstream magnetic field points toward the Sun direction in the X–Y plane so that the $\mathbf{E} = -\mathbf{V} \times \mathbf{B}$ convective electric field points in the $-Z$ direction.

magnetic field vectors super-imposed. Both Figs. 1 and 2 use the Saturn equatorial reference frame (SSQ), with $(x-y)_{SSQ}$ plane in Saturn's equatorial plane and z_{SSQ} aligned with Saturn's spin axis. The $(x\text{-axis})_{SSQ}$ is the abscissa and the $(y\text{-axis})_{SSQ}$ the ordinate with z_{SSQ} projected outward with 3D projection used. The solar direction is in the $(z-x)_{SSQ}$ plane where it is 19° below the $(x\text{-axis})_{SSQ}$. For this paper we shall primarily use a coordinate system with x pointing along the co-rotation direction, y pointing toward Saturn and z along Saturn's spin axis. In the case of T9 the spacecraft made a wake pass ~5000 km from Titan at Saturn Local Time (SLT) ~0300 h. The co-rotation direction, illuminated side of Titan and direction toward Saturn are shown. The upstream magnetic field orientation is approximately pointing toward the Sun (as a result of the strong sweepback in the field, which is typical of that SLT sector). Times of Events 1 and 2 are identified along the spacecraft trajectory. The figure also shows the CAPS field-of-view (FOV) for the (IMS) and electron spectrometer (ELS). As will be shown later, the viewing was optimal inbound, including for Event 1, but less optimal outbound for Event 2. The spacecraft was moving radially away from Saturn. During the inbound interval Cassini was probably seeing plasma coming from sunlit side of Titan, while outbound it was probably seeing plasma coming from Titan's nightside.

The T18 encounter geometry was similar to that for T9, but much closer to Titan with closest approach altitude ~950 km over the north pole as shown in Fig. 3. Local time is similar ~0300 LT so sunlit side of Titan the same as for T9, but now the spacecraft is moving toward Saturn and along Titan's terminator (i.e., in case of

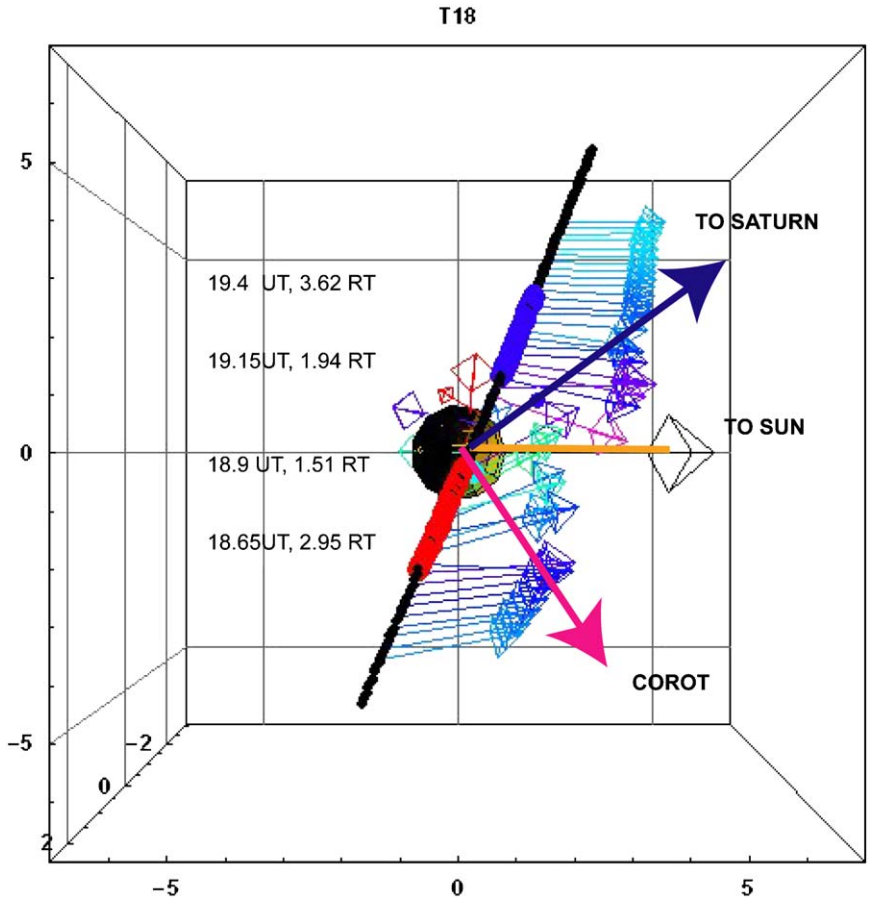

Fig. 2. Cassini T18 encounter trajectory plot in a similar format as that in Fig. 1 by Szego et al. (2007). It also shows the magnetic field vectors along the spacecraft track. The T18 encounter is much closer to Titan than T9 and is a north polar pass. The magnetic field geometry is very similar to that for T9 and is such that the convective electric field $\mathbf{E} = -\mathbf{V} \times \mathbf{B}$ points vertically downward in the $-Z$ direction. The red region indicates when perturbations in the magnetic field are observed inbound and the blue region is the same for outbound. The start–stop times and corresponding radial distances are indicated for the red and blue regions. (For interpretation of the references to color in this figure legend, the reader is referred to the web version of this article.)

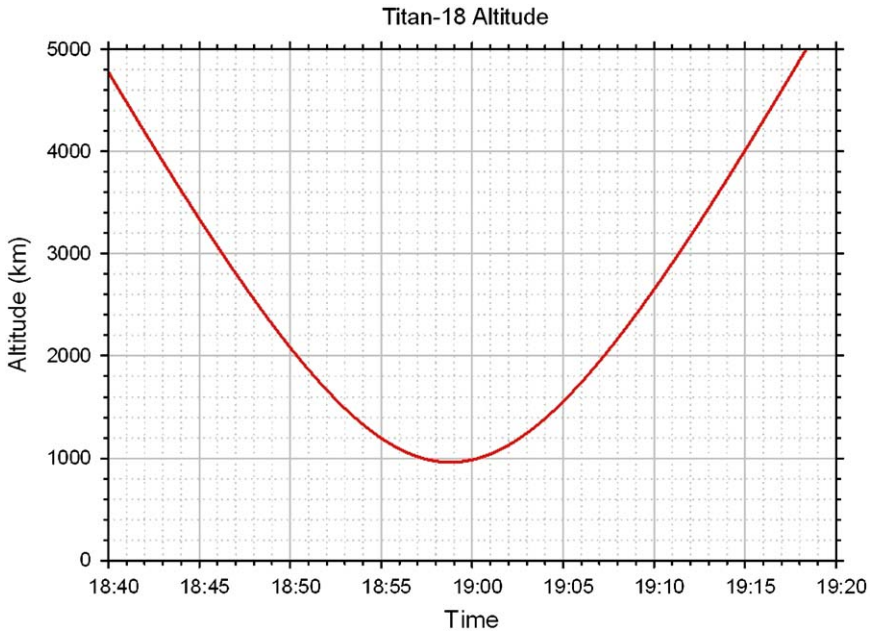

Fig. 3. Altitude plot of Cassini versus time for T18 flyby.

T9 spacecraft was moving radially away from Saturn). The upstream magnetic field alignment is close to that for T9. The red region indicates the inbound region where the field is moderately perturbed, the blue region indicates the outbound region where the field is moderately perturbed and the region in between the red and blue regions is strongly perturbed. The start and finish times and corresponding radial distances from Titan for the red and blue regions are indicated.

3. IMS data analysis issues

In this section we give a brief discussion of the data analysis that is pertinent to this paper. A more detailed description of the analysis is given in Sittler et al. (2009b). One can also refer to the Young et al. (2004) on how the CAPS instruments work. If one prefers they can skip this section, but should be considered for having a better understanding of how the results are derived.

The IMS samples singles data in eight 20° angular sectors simultaneously for each energy-per-charge (E/Q) step lasting 62.5 m s. There are 62 energy steps or levels per energy sweep which takes 4 s to acquire (time includes high voltage stepper flyback and one energy step used for background monitoring). The data are then formatted into 8 energy sweeps per instrument's internal data acquisition cycle, or A-cycle, which takes 32 s to acquire. The composition data, referred to as B-cycle data, and shown in Fig. 9, are composed of 8 A-cycles for a total of 64 energy sweeps. All eight angular sectors are summed together and every two nearby energy steps summed together (i.e., 62 E/Q steps collapsed to 32 E/Q steps) for the B-cycle data to improve signal to noise and keep telemetry rate requirements to acceptable levels. The time to acquire each B-cycle is 4 min 16 s. While the instrument is performing its E/Q sweeps the instrument's actuator is scanning both the IMS and ELS entrance system field-of-view (FOV) fans (both have collimator planes with eight angular sectors with each having FOV $\sim 8^\circ \times 20^\circ$) in windshield wiper mode at a 1°/s scan rate. The actuator scan is more than 180° wide and requires ~3 min 30 s long (i.e., we use ~6 min and 30 s for moments to ensure full coverage of velocity space is achieved) to complete [see Young et al., 2004 for instrument details]. Wilson et al. (2008) use a slightly longer accumulation period of 7 min 48 s, but for brief analysis periods such as Titan flybys the shorter period is sufficient.

The analysis procedures are similar to that used by Sittler et al. (2005, 2006, 2007) for Saturn's inner magnetosphere Saturn Orbit Insertion (SOI) period, except now generalized to take into account actuator motion and spacecraft attitude changes or rolls. Sittler et al. (2009b) gives a detailed description on how the velocity moments are computed. The main feature of this algorithm is that it is essentially model independent with the only assumption that velocity distribution function (VDF) is gyrotropic and ion beam is within instrument's 2π steradian FOV (see Sittler et al. (2009b) for details of this assumption). The approximation of gyrotropy is generally not satisfied within the pickup region around Titan but is approximately satisfied for protons. Since T9 is a proton-dominated interaction, one would expect this approximation to be generally valid for T9. Another approximation of the analysis is that the VDF is broad compared to the instrument response in energy and two angles. As discussed later, for ring or shell distribution this can be violated and corrections are required. We also have the ability to simulate data for convected bi-Maxwellians and these simulations can be generalized for ring, shell and Kappa distributions. This simulated data can be used as input for our ion moment code and look for evidence of systematic errors, Poisson noise and background effects.

The singles data, which are used as input into the ion moments program, does not have composition information. In the case of T9 and T18 composition data are available. From the composition data, W_j, described in Eq. (1), are used to weight the singles data and compute ion moments for each ion species. See Sittler et al. (2009) for a more detailed description. The weights are estimated as follows:

$$W_j(E/Q) = \frac{C_j(E/Q)}{\sum_{i=1}^{N} C_i(E/Q)} \quad (1)$$

with $C_i(E/Q)$ the accumulated counts for ion i at energy-per-charge E/Q derived from the B-cycle composition data (this data are coincidence ion counts versus E/Q and TOF channel) and N is the total number of ion species. When implementing Eq. (1) corrections must be made since the geometric factor (GF) is not the same for light ions and heavy ions. The weight files are also smoothed to remove spikes in the composition data when the counts levels are down near background levels. The heavy ions can also contribute to the light ion TOF channels ~5% level and these corrections are also made. One finds that weighting the singles data, works quite well in producing reliable ion fluid parameters for the individual ion species even when significant overlap between different species in E/Q occurs. For example, for Events 1 and 2 as discussed below, which are composed of two species (mass=17 and 29 for Event 1 and mass=1 and 2 for Event 2), yield approximately the same flow velocities $V_{17} \cong V_{29}$ when this is done (i.e., one expects both ions to be co-moving to a first approximation). Without the composition data one could not produce reliable fluid parameters for T9 using the ion moment technique. Finally, we note that when vector magnetometer data are used in this paper one uses 1 minute averages expressed in terms of our Titan coordinate system described previously with x along corotation direction, y pointing radially inward toward Saturn and z along Saturn's spin axis.

4. Observations for T9

Fig. 4 shows energy-time spectrograms of the IMS ion singles data and in Fig. 5 (see also Coates, 2009) is a revised figure from the Coates et al. (2007a) T9 paper. In Fig. 6a is shown the viewing of the IMS angular sectors with respect to the corotation direction, while Fig. 6b and c shows fan plots before and after closest approach. The oscillatory variation in Fig. 6a is due to the CAPS actuator motion, which varies from −60° to +104°. When the rotating flow is into an angular sector the angle is 180° (optimal for observing rotating flow) and when flowing out the angular sector the angle is 0° (not optimal for observing the rotating flow). The upstream flow shown in Fig. 4 near 18:00 SCET is centered ~angular sector 2, which is close to that expected for observing the rotating flow, angular sector 3, as shown in Fig. 6. After Event 2, ~19:30 SCET the flow peaks around angular sector 6, while Fig. 6 favors angular sector 8 for the rotating flow, so the flow must be deflected somewhat from the corotation direction. The gap between islands of high signal is caused by the actuator motion and the beam-like velocity distributions (i.e., confined to a few angular sectors), which can be caused by high Mach flows and/or high-temperature anisotropies.

The figures show the large-scale structure of the plasma data for T9, clearly showing high-speed flow before and after Event 1, low-speed, low-temperature and high-density flows for Event 1 and medium-speed, temperature and density for Event 2. After Event 2 the composition of higher energy ions is dominated by protons. What's also interesting is the apparent mixture of cold ionospheric ions and hot keV magnetospheric ions during the exiting boundary of Event 1. As discussed below the ionospheric

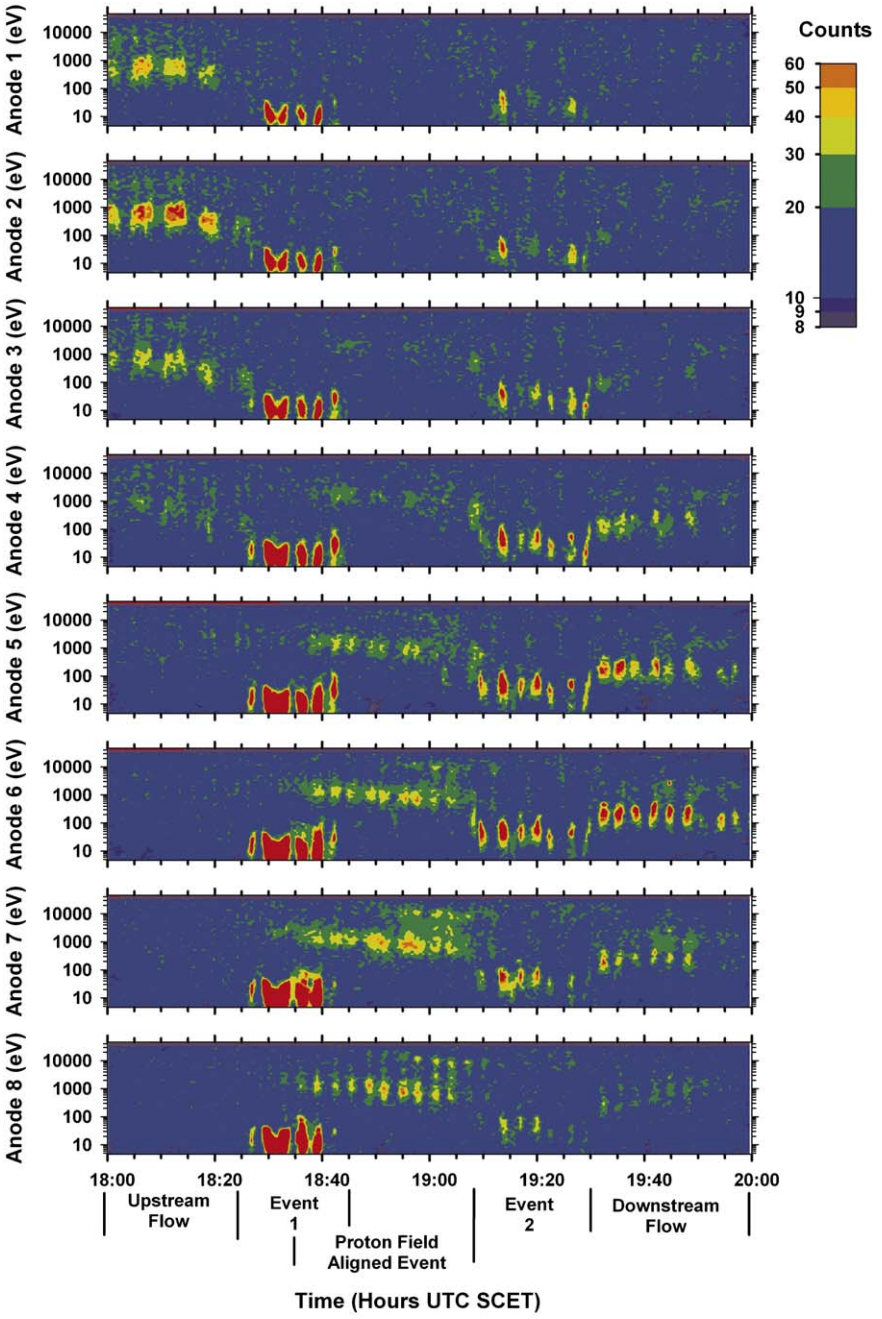

Fig. 4. Energy–time spectrogram of the CAPS IMS ion singles data for the T9 encounter period. The color bar on the right gives the ion counts versus color. The figure covers the period from 18:00 SCET to 20:00 SCET. There are eight panels for each of the instruments eight angular sectors. The time gaps between periods of signal are due to the instrument's actuator motion and the IMS collimator plane sweeping through the ion beam localized to a specific direction. Events 1 and 2 are clearly evident in the figure.

ions are moving nearly along the magnetic field away from Titan, while the hotter magnetospheric ions can inter-penetrate across field lines due to their larger gyro-radii ~900 km or ~2.5 min wide along the time axis. This is approximately what we show in Fig. 4. The electron data shows similar structure to that displayed by the ion data, but with higher sensitivity. When ion fluid parameters are discussed later in the text, comparisons with the electron fluid parameters shall be made. For event 1 one also sees a fairly wide range of angular sectors signal is observed and very little change in time series due to actuator motion. Here, flow is more transonic, but also as shown by Modolo et al. (2007a) using Langmuir Probe (LP) data the spacecraft potential for event 1 is negative, $\Phi_{SC} \sim -2$ V, which will tend to pull ions in from all directions toward instrument (i.e., flow energies ~4–7 eV). The negative spacecraft potential will also increase the calculated flow speed if not included in analysis.

In Fig. 7 we show 2D θ–φ plots of the ion counts in the local inertial frame described previously. Here, (θ,φ) are ~(90°,180°) for rotating flow, ~(90°, 90°) for outward flows and (90°, 270°) for inward flows. The white trace indicates ions moving perpendicular to the magnetic field, while the white diamonds indicate flow along the field or anti-parallel to **B**. Fig. 7a–g cover the period from 18:00 SCET to 20:00 SCET including Events 1 and 2.

At 1804:57 SCET (accumulated over 6 min 24 s period from 1804:57 to 1811:21), Fig. 7a, the signal shows the central core region of the measured ions moving perpendicular to the field and nearly isotropic in the proper frame of the ions. If these are pickup

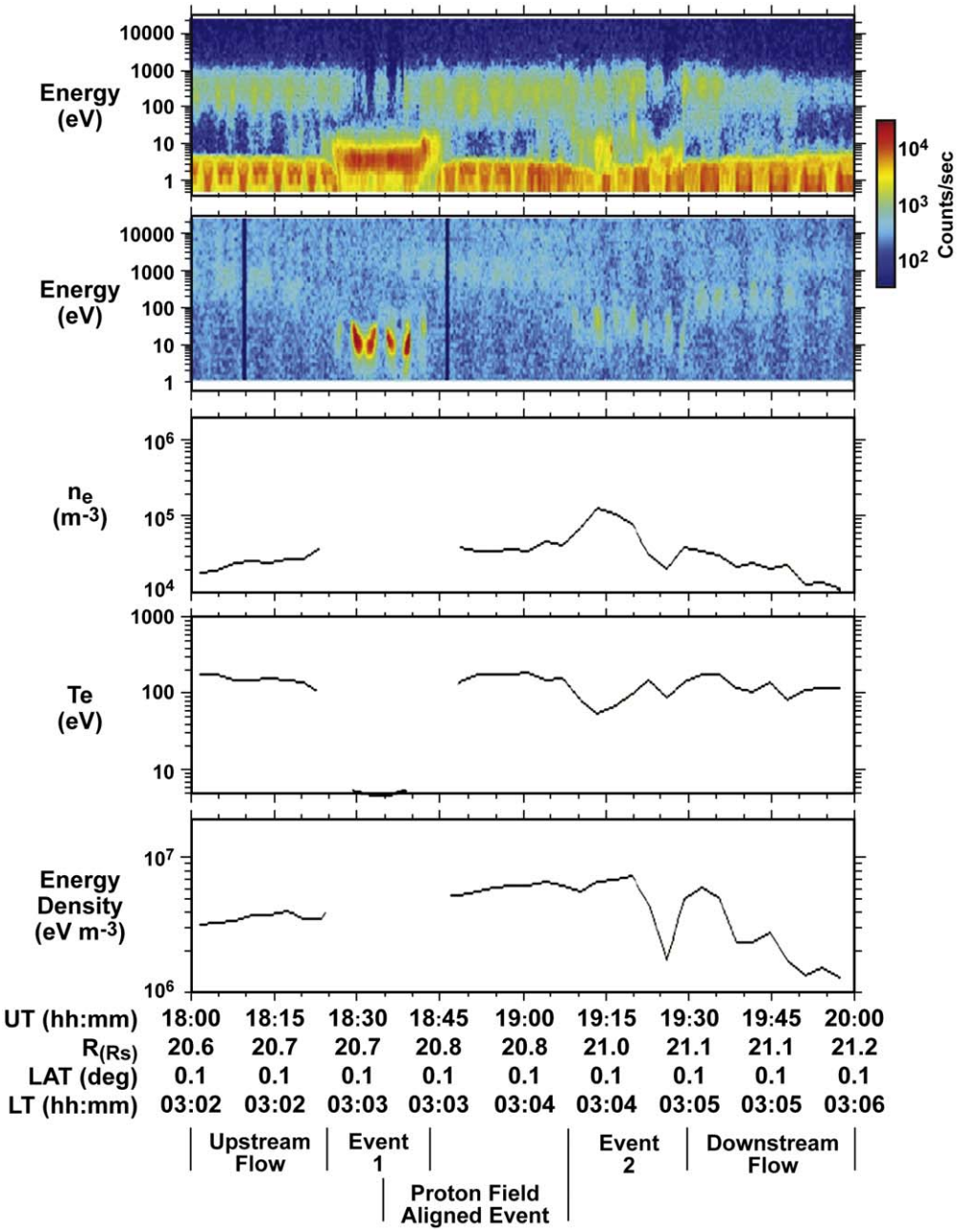

Fig. 5. Energy–time spectrogram for T9 similar to that presented by Coates et al. (2007a) in top panel and lower two panels give the electron density N_e and electron temperature T_e; they are derived from angular sector 5 measurements. Angular sector 5 looks radially away from spacecraft and thus minimizes spacecraft charging corrections. Due to a recalibration of the CAPS-ELS the densities and temperatures are revised lower than that given in Coates et al. (2007a). A similar plot with revised parameters can also be found in Coates (2009).

ions from Titan's H and H_2 exosphere (i.e., $\mathbf{E}\times\mathbf{B}$ drift $\perp$ to $\mathbf{B}$), they must have been effectively pitch angle scattered by ion cyclotron waves (throughout, pickup ions are considered those ions created and transported by the motional electric field, $\mathbf{E}=-\mathbf{V}\times\mathbf{B}$, in the collisionless plasma regions while those produced in collision and/or chemical-dominated regions are treated as elements of the local plasma fluid). The kinetic aspects shall be reserved for a later study.

Figs. 7b and c show for Event 1 the mass 17 and mass 29 ions, respectively. As expected for ionospheric ions they are very cold with temperatures ~4 eV. They also show significant temperature anisotropies $T_\perp/T_\parallel\sim 2$. The flows are almost purely in the corotation direction.

Fig. 7d shows magnetospheric protons that are very hot, moving parallel to the magnetic field, with large temperature anisotropy $T_\perp/T_\parallel\sim 2$. These ions have flow speed $V\sim 290$ km/s and temperature $T\sim 266$ eV. The process producing the large field aligned flow speeds is uncertain at this time and requires further study.

For Event 2 the ions in Fig. 7e (protons) and 7f (H_2^+) have relatively high densities ~0.16 ions/cm^3 when combined, nearly field aligned flows of speed ~53 km/s and temperatures $T\sim$12–14 eV. The ions have the temperature anisotropy $T_\perp/T_\parallel\sim 2.0$. Event 2 is clearly hotter than Event 1. Modolo et al. (2007a) LP data have shown $\Phi_{SC}\sim 0$ V for Event 2 and thus negligible correction for our analysis. For the outbound period after Event 2 as shown in Fig. 7g, the proton densities ~0.036 ions/cm^3 are much lower than in Event 2, have higher flow speeds $V\sim 160$ km/s and higher temperatures $T\sim 57$ eV. These ions are nearly isotropic in the proper frame $T_\perp/T_\parallel\sim 1.4$ and are moving perpendicular to $\mathbf{B}$ as one would expect

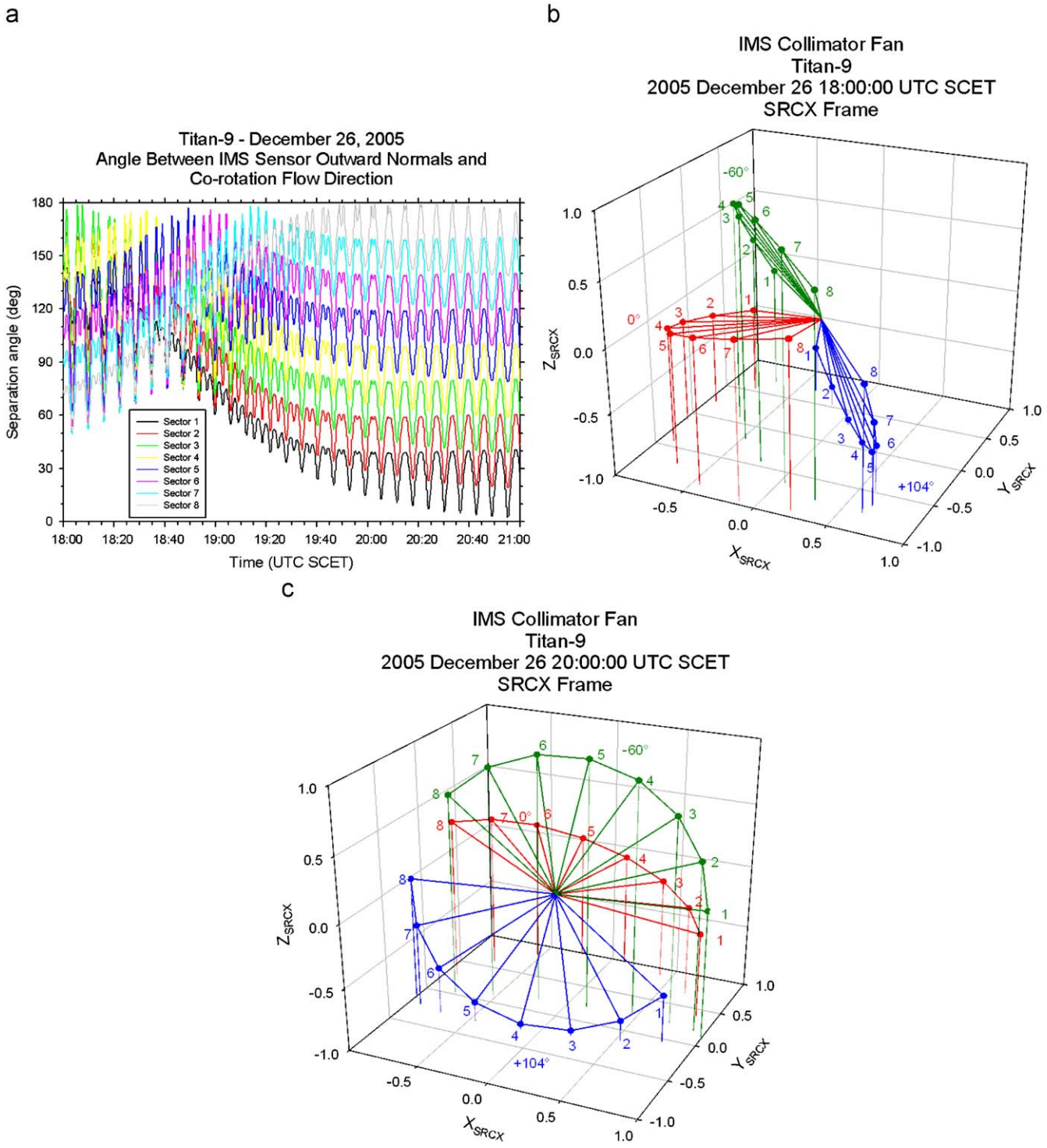

Fig. 6. Fig. 6a shows the IMS field of view (FOV) relative to the corotation direction for each of the eight angular sectors. When the angle is at 180° the rotating flow is directly into the instruments angular sector or anode of interest. The up-down motion to the curves is due to the actuator motion of the instrument. Fig. 6b shows a fan plot of the instrument's angular sectors at 18:00 h before Event 1 of T9 and Fig. 6c shows a fan plot at 20:00 h after T9 Event 2. In Fig. 4 one sees the ion beam at 18:10 SCET is centered on anode 2. Angular sector 3 is the most favored which indicates a slight deflection from corotation. For downstream flow we see beam at anode 6, which is marked by the purple curve. But as can be seen, sector 8 is closer to corotation and one therefore expects the flow to have a larger $-y$ direction. This is essentially what one gets when the singles data is used as input to the ion moments program. (For interpretation of the references to color in this figure legend, the reader is referred to the web version of this article.)

for pickup ions. Similar observations were observed for the upstream flow.

In Fig. 8 are shown the ion fluid parameters and magnetic field for T9 derived from velocity moments of the CAPS IMS singles data. The top panel for Fig. 8 has ion density, second panel down is ion temperature in eV, third panel down is ion flow velocity vector and bottom panel is magnetic field vector and magnitude in Titan coordinates with B_X in blue, B_Y in red, B_Z in green and B in black.

Fig. 10a shows B-cycle ion counts versus time-of-flight (TOF) for all $E/Q \sim 12.4$ eV/e in the Event 1 period. Fig. 10b shows a single B-cycle spectrum for Event 2 period, not previously identified,

that shows the first evidence of mass 16 ions. In order to extract the particular ion from the data, one sums over all $E/Q \leq 50$ eV and sums over eight nearby TOF channels. So, there is now evidence of some heavy ions during Event 2 with low energy pickup ions indicating source near magnetopause region where flow is significantly mass loaded. If pickup ions the mass/charge (M/Q) assignment of 16 for CH_4 is more likely. If these ions are of ionospheric origin then why no evidence of $M/Q \sim 29$ ions? Fig. 10a shows that Event 1 is composed of ionospheric plasma due to presence of both $M/Q \sim 17$ and $M/Q \sim 29$ ions.

Fig. 11 shows for T9 the angle between the estimated ion flow velocity vector and the local magnetic field direction for the same time period covered in Fig. 8. This plot shows that for both upstream and downstream periods the protons are moving at right angles to **B,** which as previously discussed, is consistent with these protons being pickup ions from Titan's extended H and

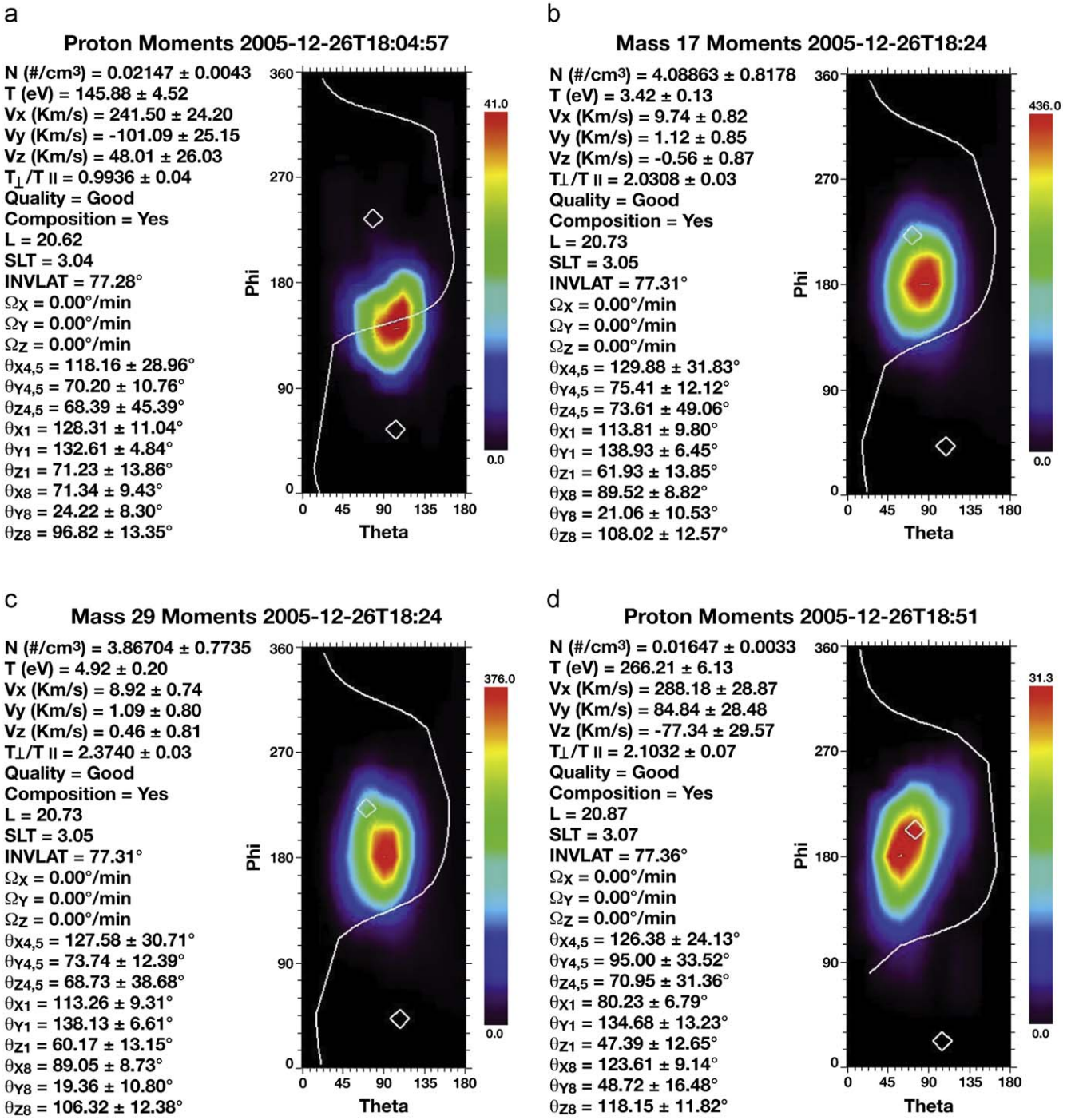

Fig. 7. Shows theta–phi plots as described in the main text. Fig. 7a is the upstream flow, Fig. 7b is T9 Event 1 mass 17 ions, Fig. 7c is T9 Event 1 mass 29 ions, Fig. 7d is the energetic field-aligned event between Events 1 and 2 of T9, Fig. 7e is protons for Event 2 of T9, Fig. 7 f is H_2^+ ions for Event 2 of T9 and Fig. 7g is the downstream flow after Event 2 of T9. The solid white line indicates ion velocities perpendicular to magnetic field and the white diamonds indicate either ion velocities along magnetic field or anti-parallel to magnetic field. (Ω_X, Ω_Y, Ω_Z) are the spacecraft roll angular velocities about its x-, y- and z-axis. This is used to tell us when the spacecraft is rolling or performing a maneuver. The angles $\Theta_{X4,5}$, Θ_{X1}, and Θ_{X8} give the average angle $\pm$ one sigma variations between angular sectors (4,5), 1 and 8 relative to the X-axis of our Titan coordinate system. The same can be said for the Y and Z components. One uses this information to ascertain the viewing geometry for observing the rotating flow about Saturn.

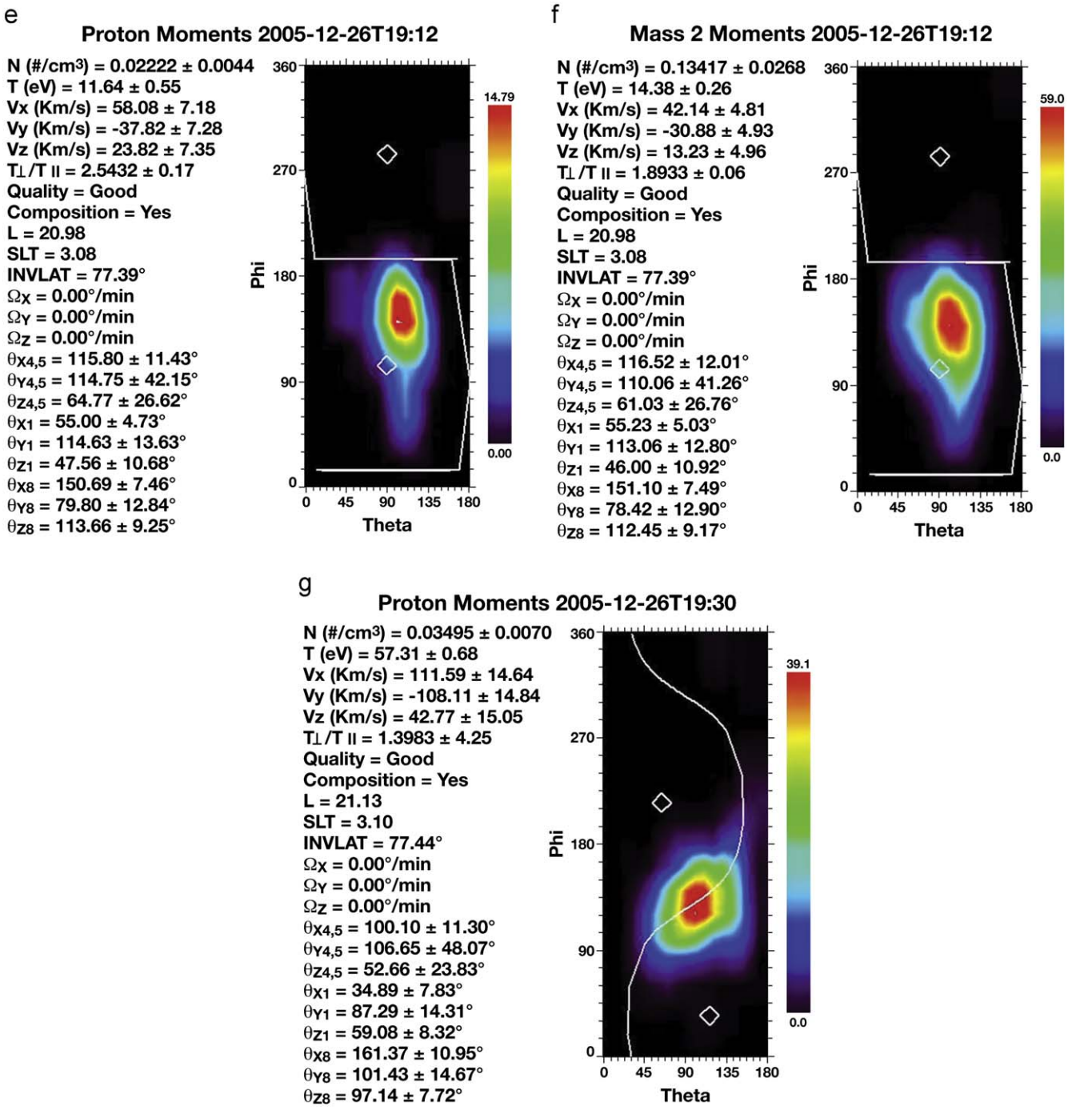

Fig. 7. (*Continued*)

H_2 corona, that are **E** × **B** drifting relative to **B.** Events 1 and 2 are moving ~30° relative to **B** and away from Titan, while for period between Events 1 and 2, magnetospheric protons are moving at higher energies along the magnetic field. For the upstream period (see Fig. 8) one sees an anti-correlation between V_X and B_X, which could mean one is seeing evidence of Alfven waves moving along the local magnetic field. Using the proton density N_P~0.006 ions/cm^3 and B~6 nT the Alfven speed V_A~1690 km/s and for δB_X~1 nT we estimate $\delta V_X = (\delta B_X/B)V_A$~282 km/s. The observed δV_X~50 km/s indicates the waves are not purely Alfvenic or that heavier undetected ions are present (there are mass 2 ions present at 12% abundance relative to protons).

4.1. Upstream flow

For the period 17:00–18:20 the spacecraft is in the upstream plasma and as shown in Fig. 9, the composition is nearly all protons with some mass 2 ions present. The ion densities in Fig. 8 for the upstream flow are ~0.006 protons/cm^3, and proton temperatures are ~30–100 eV from 17:00 to 18:00, while from 18:00 to 18:20 the proton densities are ~0.02–0.03 protons/cm^3 and T_P~200 eV. For the latter period the plasma electron densities N_e~0.03 el/cm^3 and temperatures T_e~200 eV are very close to that for protons as shown in Fig. 5 (revised from that reported by Coates et al., 2007a). Fig. 9a also shows two peak spectrum for protons that does not appear to be due to time aliasing.

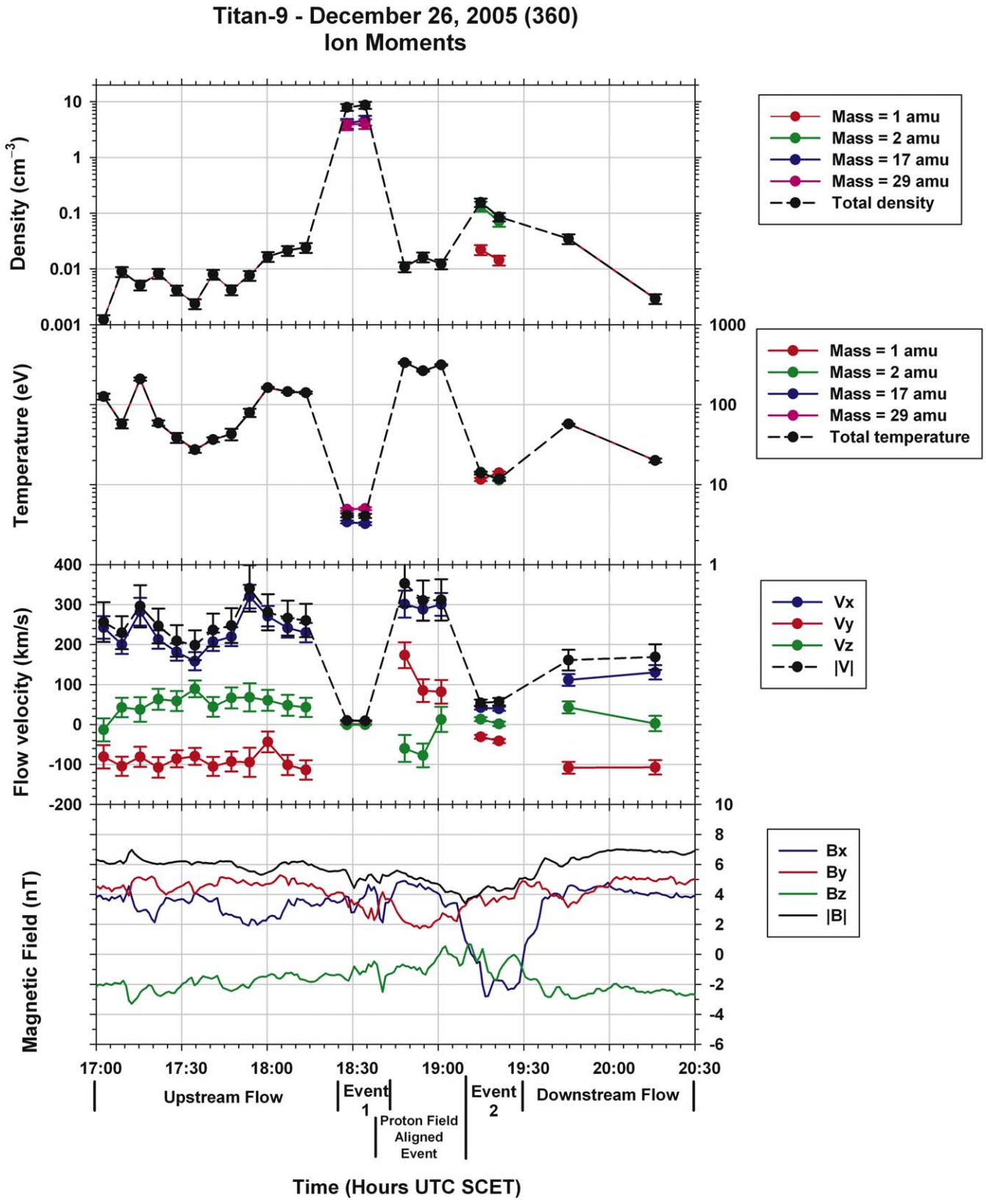

Fig. 8. T9 ion moment results using VDFs similar to those shown in Fig. 7 along with magnetometer data are shown. The top panel is the ion density, 2nd panel down is the ion temperature and 3rd panel down in the ion flow velocity vector (V_X (blue), V_Y (red), V_Z (green) and total speed (black)). The bottom panel is the magnetic field vector measurements. Due to the slow actuator motion, ~1°/s, it takes ~6.5 min to make one complete measurement of the ion velocity space (i.e., code can be optimized to reduce this time period to less than 4 min). The dots indicate data points with the lines only used to help follow the trend of the data. The time resolution of the magnetometer data is 1 min. Keys for the four panels are shown on the right. This plot covers the period from 17:00 SCET to 20:30 SCET. One sigma error bars are shown for the ion data. (For interpretation of the references to color in this figure legend, the reader is referred to the web version of this article.)

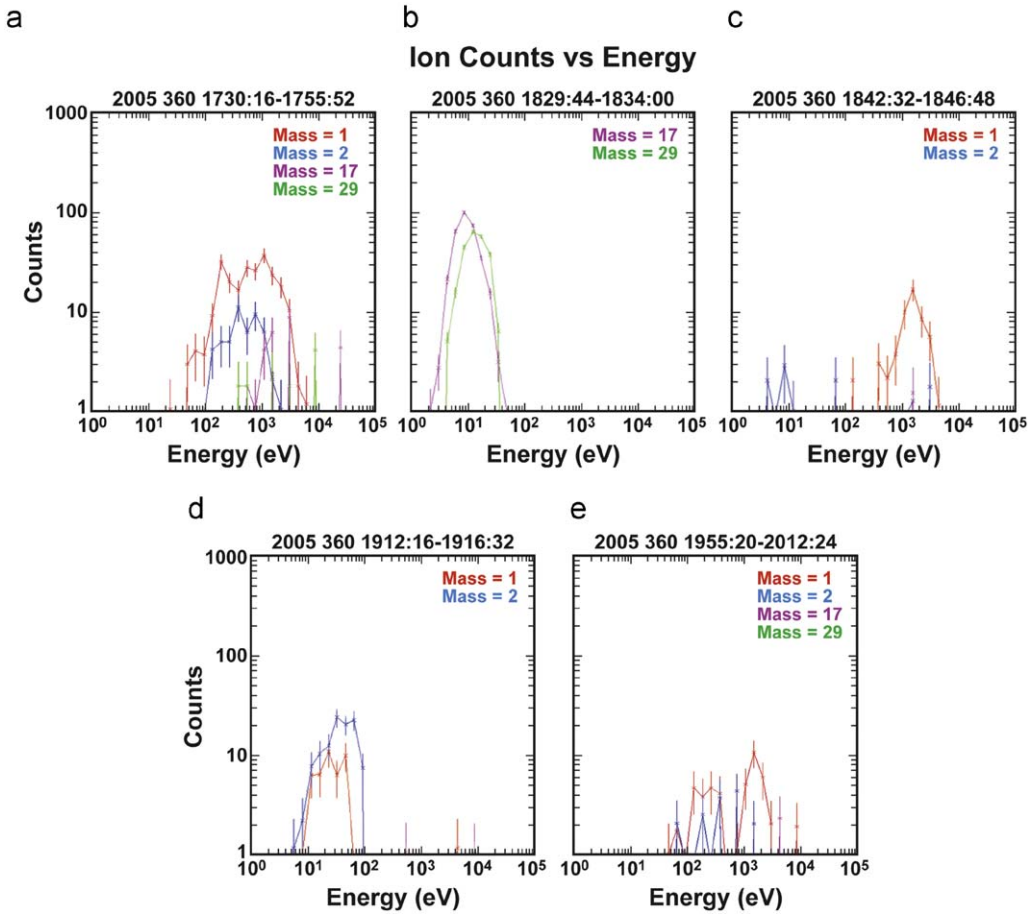

Fig. 9. This figure shows the ion composition data for various periods of interest. The data are ion counts versus energy-per-charge (E/Q). The ion counts for each mass group are computed by summing the counts within the time-of-flight (TOF) peak position of a particular ion at specific incident energy (i.e., peak position energy dependent). The TOF window is defined by the ions TOF peak position $\pm 2\sigma$ where σ is the 1/e width of the peak in TOF space. Red is used for protons, blue for H_2^+, purple for mass 17 and green for mass 29. Panel a is for the upstream period before Event 1, panel b is for Event 1, panel c is for the high-speed field-aligned proton event between Events 1 and 2, panel d is for Event 2 and panel e is for the downstream event after Event 2. (For interpretation of the references to color in this figure legend, the reader is referred to the web version of this article.)

Preliminary simulations indicate that shell distributions could produce such an energy dependence. The upstream flow velocity is found to be primarily azimuthal with $V_X \sim 250$ km/s, which is faster than co-rotation speeds ~ 200 km/s. It also exhibits wave-like perturbations, $\delta V_X \sim 50$ km/s, which anti-correlates with the fluctuations in the magnetic field $\delta B_X \sim 1$ nT with periods ~ 40 min. If one uses estimated Alfven speed from above parameters $V_A \sim 1690$ km/s and assumes waves in bounce resonance with Saturn's ionosphere (i.e., waves reflect at ionosphere) with path length $\sim \pi \times 20 R_S$ one gets bounce period ~ 37 min very close to our observations (see Glassmeier, 1980).

In addition, there are significant outward radial velocities away from Saturn $V_Y \sim -100$ km/s and $V_Z \sim +50$ km/s. When these are combined with V_X the flow is a right angles to the magnetic field. One interpretation is that the protons are pickup ions $\mathbf{E} \times \mathbf{B}$ drifting perpendicular to $\mathbf{B}$. As discussed previously, the protons are nearly isotropic implying pitch angle scattering has occurred, but simulations indicate can be in form of a thin shell VDF. When one compares plasma pressure with magnetic field pressure one finds $P_{\mathrm{plasma}} \sim n_e k(T_p + T_e) \sim 1.9 \times 10^{-11}$ ergs/cm^3, $B^2/8\pi \sim 1.4 \times 10^{-10}$ erg/cm^3 and $\beta \sim 0.14 \ll 1$. When one compares the flow energy density with the magnetic field energy density $1/2\rho V^2 \sim 1.6 \times 10^{-11}$ ergs/cm$^3 \ll B^2/8\pi$ and is ~ 10 times less than the field energy density. So, we essentially have a low beta plasma interaction, which is consistent with a relatively low mass flux impinging upon the upper atmosphere of Titan. A relatively higher beta plasma impinged upon Titan's atmosphere during the TA flyby that was due to the presence of the hot, heavier ion O^+. Such heavy ions have been observed to penetrate well into Titan's thermosphere (Hartle et al., 2006d) while most of the protons are deflected around the obstacle. In these cases relatively larger energy inputs to Titan's upper atmosphere are then expected from the higher beta magnetospheric plasma.

4.2. Event 1

In Fig. 8 only two data points are shown for Event 1, which actually extends from 18:20 to about 18:40. The third point in the period did not quite meet our requirements for a full actuator scan and there was some time aliasing with the high-speed proton event sandwiched in between Events 1 and 2. The composition for Event 1 is given by Fig. 9b, which shows overlapping peaks in energy for $M/Q \sim 17$ and $M/Q \sim 29$ for energies between 2 and 50 eV. Smaller proton and H_2^+ ion peaks at lower energies are present but not shown. The $M/Q \sim 17$ peak is wider than the $M/Q \sim 29$ peak with the $M/Q \sim 29$ peak shifted to a slightly higher energy than the $M/Q \sim 17$ peak by the ratio 29/17 as one would expect if they were co-moving. This overlap between peaks does not allow one to perform velocity moments for each ion separately

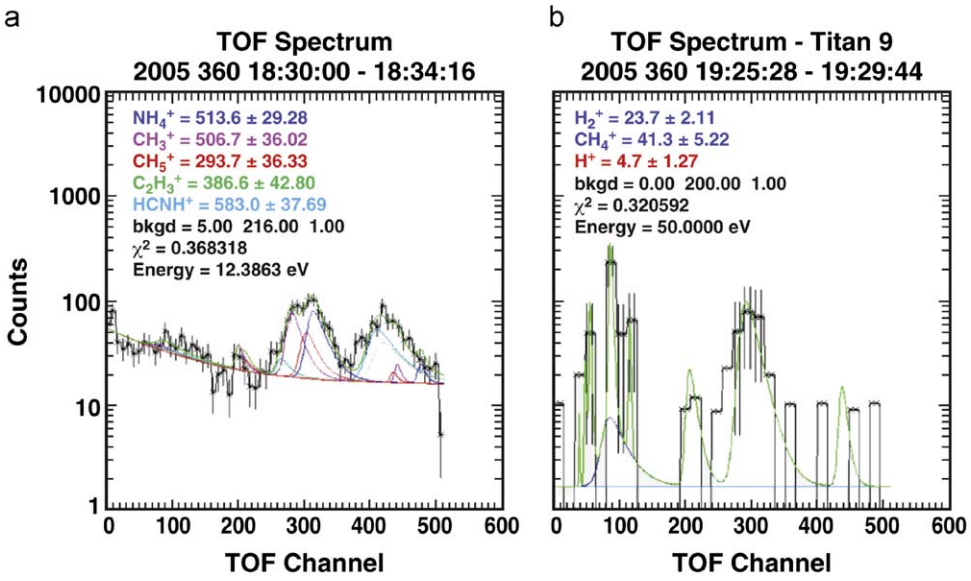

Fig. 10. Panel a is a plot of the composition data during Event 1 and the signal is for energies 12.4 eV/e. The format is counts versus time-of-flight (TOF). One shows this as evidence for an ionospheric composition signature for Event 1. This spectrum can be modeled with CH_3^+, CH_5^+ and NH_4^+ (mass 17) and $HCNH^+$ and $C_2H_5^+$ (mass 29) as the dominant ions, but cannot exclude mass 16 (CH_4^+) or mass 28 (N_2^+). Since the electrons appear more like ionospheric photoelectrons one is likely seeing ionospheric ions and not pickup ions. The presence of NH_4^+ gives further evidence of ionospheric source. Panel b is same format but now for Event 2 with counts summed over all energies less than 50 eV. In order to reveal presence of heavy ions 8 nearby TOF channels have been summed together and then divided by 8 to get average counts. The data shows heavy ion component which is interpreted to be CH_4^+ pickup ions and absence of mass 29 ions, although mass 17 (CH_5^+) cannot be excluded. In both panels a and b, no O-fragment is observed so a magnetospheric component with water group ions can be excluded.

using the singles data alone. In order to extract fluid parameters from the singles data, the composition data shown in Fig. 9b are used to weight the peaks. This technique is discussed in Sittler et al. (2009b). When this is done, one gets roughly the same flow velocity vector for both ion species.

In Fig. 10a is shown the ion composition data for Event 1, but now showing ion counts versus time-of-flight (TOF). The signal was acquired from 18:30:00 to 18:34:16 for ion transition energy ~12 eV so both mass peaks are shown. It shows two clear peaks, one centered on mass 17 and the other around mass 29. The identification is primarily guided by photochemical models by Cravens et al., (1997, 2004) and Vuitton et al. (2007). We see evidence of CH_3^+, CH_5^+ and NH_4^+ for the mass 17 peak and $HCNH^+$ and $C_2H_5^+$ for the mass 29 peak. Here, $CH_3^+ \approx NH_4^+$ and $CH_5^+ \sim 1/2 CH_3^+$. For mass 29 $HCNH^+ > C_2H_5^+$. At energy ~8.4 eV one just sees the mass 17 peak and the $CH_3^+ \approx CH_5^+ \approx NH_4^+$ counts and the total counts are higher. In the Vuitton et al. (2007) photochemical model they get $[CH_3^+] \sim 9.5$ ions/cm^3, $[CH_5^+] \sim 30$ ions/cm^3 and $[NH_4^+] \sim 15$ ions/cm^3. For the mass 29 peak, if one goes to energy ~17 eV the total counts peak for mass 29 with mass 17 almost at background levels. Here, $HCNH^+ \approx C_2H_5^+$ in total counts. Vuitton et al. (2007) $[HCNH^+] \sim 460$ ions/cm^3 and $[C_2H_5^+] \sim 200$ ions/cm^3. The relative abundance of the mass 17 sub-species and for mass 29 subspecies are similar to the model results by Vuitton et al. (2007) which was done for heights ~1100 km. But Fig. 10a shows mass 17 abundances similar to mass 29 abundances. It must be remembered the ionospheric plasma is being observed at heights when collisions are less important, and if the ions are pulled out of the ionosphere by the polarization electric field (Hartle et al., 2008a, b), then it will be harder to remove the heavier ions so the mass 29 ions are expected to be less abundant than that at 1100 km altitude. The ions chosen for the analysis of the TOF data are not necessarily unique but do provide a good representation of the data. The presence of both mass 17 and mass 29 ions is good evidence for ionospheric ions, although CH_4^+ and N_2^+ cannot be eliminated as pickup ions within Titan's topside ionosphere (i.e., CAPS IMS cannot uniquely separate the two interpretations at this time, but since spacecraft is within Titan's induced magnetotail, Coates et al., 2007a, b identified ionospheric photoelectrons for same time period and the photochemical models noted above favor CH_5^+ and $C_2H_5^+$ identifications we feel mass 17 and 29 is the more likely identification).

Fig. 8 also shows that the ions have about the same density $n_{17} \sim n_{29} \sim 3.96$ ions/cm^3, nearly same temperature $T_{17} \sim 3.4$ and $T_{29} \sim 4.9$ eV with mean temperature $T \sim 4.2$ eV. In both cases the flow speeds are ~9 km/s and the combined densities ~7.93 ions/cm^3. These total ion densities are very close to the Langmuir Probe (LP) electron densities ~10 el/cm^3 reported in Bertucci et al. (2007) and Modolo et al. (2007a). When one makes rough correction for spacecraft potential $\Phi_{SC} \sim -2$ V as reported by Modolo et al. (2007a) LP data then lower flow speeds ~7 km/s are expected. Modolo et al. (2007a) estimated the heavy ion flow speeds for Event 1 to be ~10–20 km/s, which were reasonably close to our estimate ~7–9 km/s. The LP data gave ion temperature upper estimates ~15–60 eV for assumed ion mass ~28 amu, which is much larger than the temperatures estimated here. In a qualitative sense we are in agreement with all the other data sets and are in good agreement when it comes to ion densities for which the LP are expected to yield accurate estimates. Therefore, the analysis presented here provides accurate fluid parameters for Event 1. Finally, when one combines the total ion densities and ion velocities one gets an ion flux $\sim 7 \times 10^6$ ions/cm^2/s, which is very close to the inferred ion outflow $\sim 10^7$ ions/cm^2/s by Hartle et al. (2008a,b) using TA data. This inference was based on the LP electron density and pressure gradients at the topside ionosphere (see Wahlund et al., 2005) and using the electron momentum equation for the polarization electric field $EPOL \sim -(1/n_e)\nabla P_e$. The idea was originally proposed by Hartle and Grebowsky (1995) for Venus. Referring to this, Coates et al. (2007a, b) did mention the importance of an electric field for Event 1 with regard to plasma escape from the ionosphere. Here, the acceleration by this electric field is more than an order of magnitude greater than that due to gravity for $M/Q \sim 28$ ions. The outflow speed at the top of the ionosphere was estimated to be ~1 km/s, so the ions must have experienced considerable acceleration by the time

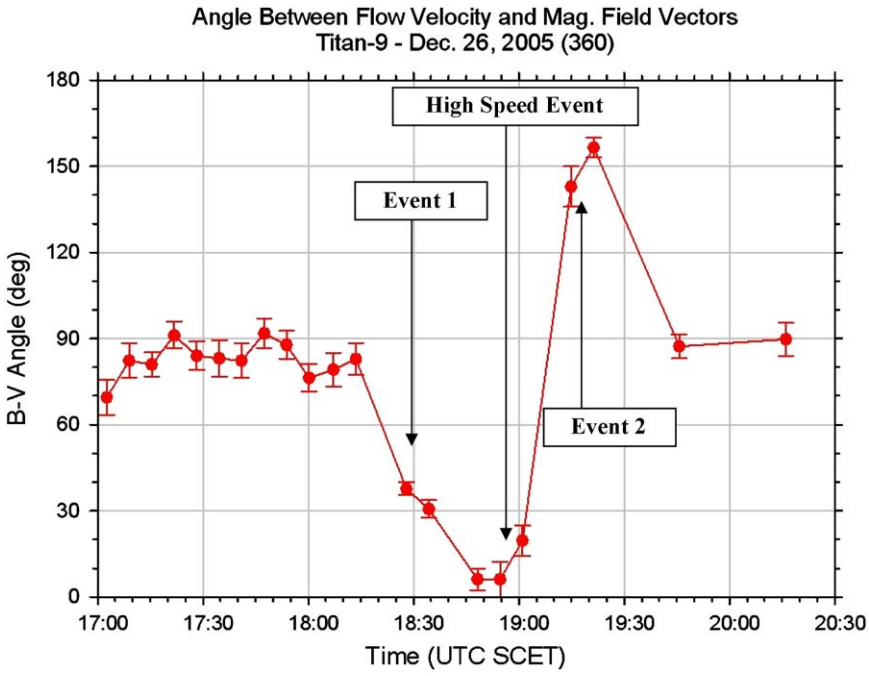

Fig. 11. This figure shows the angle between the observed flow velocity and local magnetic field direction for T9. It shows for both upstream and downstream flows the flow is perpendicular to **B**. For Events 1 and 2 the flow is $\sim 30^\circ$ from field aligned and is moving away from Titan. In the case of Event 2 the field direction is reversed so one gets angles $\sim 150^\circ$.

they reached T9 altitudes. One might ask why TA and T9 are the same, but this mechanism is primarily driven by the ionospheric electrons heated by the photoelectrons for both encounter periods (see Cravens et al., 2005). Referring to Fig. 11 one can see that these ions are moving within 30° of the local magnetic field direction, moving within 10° of the corotation direction and moving away from Titan. The magnetic field is probably not channeling the flow of these ions, since the plasma $\beta \sim 1$ and ion ram energy density ~ 2 times the field energy density (i.e., $B \sim 5$ nT so $B^2/8\pi \sim 10^{-10}$ dyne/cm^2, $(n_{17}kT_{17}+n_{29}kT_{29}) \sim 10^{-10}$ dyne/cm^2 and flow energy density $1/2\rho V^2 \sim 2 \times 10^{-10}$ erg/cm^3). It is also important to note that the Event 1 heavy ions are considerably hotter, $T_{ION} \sim 4.2$ eV (i.e., 50,000 K) than their expected ionospheric values (i.e., collision dominated region) with $T_{ION} < 1.73 \times 10^{-2}$ eV or 200 K. So, during their acceleration to higher altitudes they must have experienced considerable heating.

This outflow of ionospheric ions for Event 1 was inferred from the electron data reported by Coates et al. (2007a, b). They reported evidence of field aligned flow of ionospheric electrons from Titan. Also, the magnetometer data showed that Event 1 was magnetically connected to Titan (Bertucci et al., 2007), further supporting the claim here that outflowing ionospheric ions from Titan are being observed (see previous discussions on ion composition). Coates et al. (2007a, b) also reported seeing a localized electron energy peak around 22–24 eV, which is consistent with photoelectron production from the ionization of N_2 in Titan's ionosphere due to the solar He 304 nm line. In summary all the relevant data sets are consistent with the interpretation of heavy ion ionospheric plasma escaping down Titan's induced magnetotail Event 1 lasted ~ 24 minutes so with spacecraft velocity relative to Titan ~ 6 km/s translates to cross-section 8640 km or cross-sectional area of 5.9×10^{17} cm^2. With observed outflow $\sim 7 \times 10^6$ ions/cm^2/s we estimate total ion loss $\sim 4 \times 10^{24}$ ions/s. Sillanpaa et al. (2006) using a hybrid simulation studying ion escape from Titan's ionosphere, estimated ion loss rates $\sim 1.5 \times 10^{25}$ ions/s about 4 times that estimated here. Their approach was different from that used by Hartle et al. (2008a,b) with photo-ionization being the primary source of ionospheric ions.

4.3. High-speed field aligned proton event

In between Events 1 and 2 the plasma data shows protons moving along the magnetic field direction with speeds $V \sim 300$ km/s with the azimuthal component dominant, but with significant $V_Y \sim 100$–200 and $V_Z \sim -80$–0 km/s components. See Fig. 1 to help visualize geometry of encounter for this particular period. The variations, $\boldsymbol{\delta V}$, seem to be responding to magnetic field variations, $\delta \mathbf{B}$, in such a way that the flow remains field aligned. This can be seen in Fig. 11. The composition data in Fig. 9c shows only protons with flux peaking at ~ 2 keV. The high speed could be caused by draped field lines becoming detached from Titan's topside ionosphere so that the field tension can accelerate the flow to speeds greater than corotation (see Hartle et al., 2006a, b for TA). But it is not clear that the flow would still be field aligned. Coates et al. (2007a, b) noted that during this period (18:40–19:10 SCET) the spacecraft is probably not magnetically connected to Titan, which favors the interpretation of disconnected field lines. The plasma density is similar to that for the upstream flow with densities ~ 0.015 ions/cm^3 but considerably hotter with proton temperatures $T_{ION} \sim 267$ eV. Such high temperatures translate to thermal speeds ~ 225 km/s and sonic Mach numbers $M_S \sim 1.5$. The electron densities from ELS $n_e \sim 0.03$ el/cm^3 are close to the proton densities with the electron temperatures somewhat lower $T_e \sim 200$ eV (i.e., high temperatures exclude ionospheric source). The proton temperature anisotropy is $T_\perp/T_\parallel \sim 2.0$. Szego et al. (2007) reported that the viewing of the flow became less favorable during this time period, but the moments algorithm is still able to produce accurate fluid parameters. This is because of its ability to fill up the unmeasured phase space as discussed in Sittler et al. (2009b). This feature

cannot be reproduced by the hybrid simulations of Modolo et al. (2007b) who only attempted to match density, magnetic field and composition features of the data reported by Modolo et al. (2007a), Bertucci et al. (2007) and Szego et al. (2007). The high flow speeds may be an important discriminator in future hybrid simulations of the interaction.

The field-aligned properties of the flow could be serendipitous or an indication of field-aligned acceleration as previously discussed. A number of possibilities can only be speculated at this time and is beyond the scope of this study. More detailed kinetic modeling of Titan's interaction will be required to understand this observation.

4.4. Event 2

During Event 2 the ion composition shown in Fig. 10d has a significant H_2^+ component along with some H^+ ions as previously reported by Szego et al. (2007). The total ion density $n_{ION} \sim 0.18$ ions/cm^3 is very close to the ELS estimate of 0.2 el/cm^3 and lower than that reported by the LP data in Modolo et al. (2007a) at about 19:15 SCET with $n_e \sim 1.0$ el/cm^3. As discussed previously in Fig. 10b it is seen that, a mass 16 ion was briefly detected for one B-cycle, but cannot account for the higher density point reported by Modolo et al. (2007a), since it occurs at a different time. However, it does coincide with their data gap 19:20–19:30. The results from the LP data analysis by Modolo et al. (2007a) were not extended to the end of Event 2. They covered 1920–1930 SCET, while our analysis shows Event 2 extending to ~1935 SCET. In the case of Event 2, our ion temperatures are ~12–15 eV and flow speeds ~53–73 km/s. The Modolo et al. (2007a) LP data, when assuming an ion mass ~2, gave an upper estimate for the ion temperatures ~100 eV and flow speeds ~100 km/s. So, in a qualitative sense their flow speeds are in agreement, but their ion temperatures are considerably greater than ours. When comparing to the ELS fluid parameters, the electron density is ~0.2 el/cm^3 and electron temperature $T_e \sim 60$ eV.

Fig. 11 shows that the flow is moving ~30° from the field-aligned direction and moving away from Titan. We interpret Event 2 similar to that by Modolo et al. (2007b) where we are seeing draped field lines scavenging H_2^+ ions (see Dobe et al., 2007) from the inflated outer boundary of the induced magnetosphere of Titan. H_2^+ can be produced by EUV ionization, which tends not to dissociate the H_2 and the same is true for charge exchange collisions, while electron impact ionization will tend to dissociate the H_2 and produce pickup H^+ ions and H_2^+ ions but at a lower rate (see Sittler et al., 2005 for cross-sections). Since the upstream flow is dominated by H^+ ions the charge exchange rate is $\sim 1.7 \times 10^{-10}$ ionizations/s, while the photoionization rate is $\sim 5.9 \times 10^{-10}$ ions/s. The electron impact ionization rate to make H^+ from H_2 is estimated to be $\sim 5 \times 10^{-9}$ ionizations/s (cross-sections and rates can be found in Sittler et al., 2005). Since, H_2^+ tends to dominate, the observed composition does not favor electron impact ionization, so photoionization must dominate. Therefore, we propose that these ions most likely form inside the induced magnetopause boundary where magnetospheric electrons are expected to have limited access. We will return to this issue when discussing T18 plasma and field data.

The detection of mass 16 ions for Event 2 are interpreted as pickup CH_4^+ ions and their low energy indicates they form near the magnetopause boundary where the flow stagnates and pickup energies are low. The CH_4^+ ions are observed below 50 eV with max pickup velocity of ~24 km/s.

Combining the density and velocity data for the light ions the outflow flux is $\sim 10^6$ ions/cm^2/s. Modolo et al. (2007a) estimated an outflow ~ 2–7×10^{25} ions/s for cylindrical tail with radius ~2.5 $R_T \sim 6400$ km equivalent to an ion flux ~ 1.5–5.4×10^7 ions/cm^2/s. For Event 1 we estimated an ion flux $\sim 7 \times 10^6$ ions/cm^2/s so this gives a mean ion outflow $\sim 8 \times 10^6$ ions/cm^2/s, which is close to their lower estimate. This estimate is important since it represents a continual loss of ionospheric plasma to Saturn's magnetosphere and must be continuously replaced by the ionospheric sources, which in the case of T9 are expected to be dominated by solar EUV (see Cravens et al., 2005 and Johnson et al., 2009).

4.5. Downstream flow

This region shows ion flow dominated by protons (see Fig. 9e) with flow velocities nearly perpendicular to **B** (see Fig. 11) and flow speeds ~161 km/s (80% of corotation) (see Fig. 8). H_2^+ ions peaking about 200 eV come and go in the mass spectra, while the two peak structure for protons is more time invariant. It cannot be ruled out that the dual proton peak in Fig. 9e is aliased in time or a mixture of different flux tubes, some low energy and others higher energy. Therefore, this period is more difficult to quantify and may require a more in depth analysis in the future. The proton densities are ~0.012 protons/cm^3 and proton temperatures ~57 eV. The electron densities are ~0.01 el/cm^3 and electron temperature $T_e \sim 100$ eV. These plasma parameters are very similar to that observed during the inbound approach to Titan. The temperature anisotropy as shown by Fig. 7g, is $T_\perp/T_\parallel \sim 1.4$, which indicates that the protons are nearly isotropic. As with the inbound flow one is probably observing pickup ions from Titan's extended H and H_2 corona and with $\mathbf{E} \times \mathbf{B}$ drift perpendicular to **B**. Pitch angle scattering must be occurring since a ring distributions ($T_\perp/T_\parallel \gg 1$) is not observed. The two peak structure in energy in Fig. 9e could indicate shell distribution. The plasma pressure is $n_e k(T_P + T_e) \sim 2.5 \times 10^{-12}$ dyne/cm^2 while magnetic field pressure $B^2/8\pi \sim 1.95 \times 10^{-10}$ dyne/cm^2 so the plasma beta $\beta \sim 0.01 \ll 1$.

5. Complementary observations from T18

We now consider the T18 flyby, shown in Fig. 2, which has an interaction similar to T9. Since the spacecraft comes much closer to Titan, as shown in Fig. 3, it allows us to sample the induced magnetosphere and its boundaries at lower altitudes. The large-scale magnetic field of the magnetosphere has a magnetodisk geometry (see Bertucci et al., 2009), which can be seen in Fig. 12 by the large positive B_Y component (or $B_R < 0$), small positive B_X component or B_φ (i.e., indicates sub-corotating flow) and small negative B_Z component. This field topology extends for many hours before and after closest approach. Therefore, like T9, Titan is below the current sheet of the magnetosphere. Using the same approach as T9 to evaluate the moments leads to ion densities that are about 10 times larger than the observed electron densities $N_e \sim 0.003$ el/cm^3 shown in Fig. 16 with electron temperature $T_e \sim 100$ eV. Like the T9 flyby, the corresponding upstream flow velocities are also perpendicular to **B**. The primary difference is that the upstream flow has a significant H_2^+ component. This is shown in the ion composition energy spectrum plots in panel (a) and (b) of Fig. 13 for the upstream flow and the downstream flow, respectively. Fig. 14 shows the IMS ion singles data in energy–time spectrogram format with each panel representing one of the eight angular sectors or anodes of the IMS. Both Figs. 13 and 14 shows the inbound period peaking around a few hundred eV, while outbound external flow peaks around 1–3 keV and thus higher flow speeds.

In Fig. 15a we show the IMS FOV relative to the corotation direction with same format as Fig. 6a for T9. Fig. 3 shows the spacecraft altitude versus time for T18. Since, the magnetic field is nearly aligned along the solar direction and thus 45° relative to

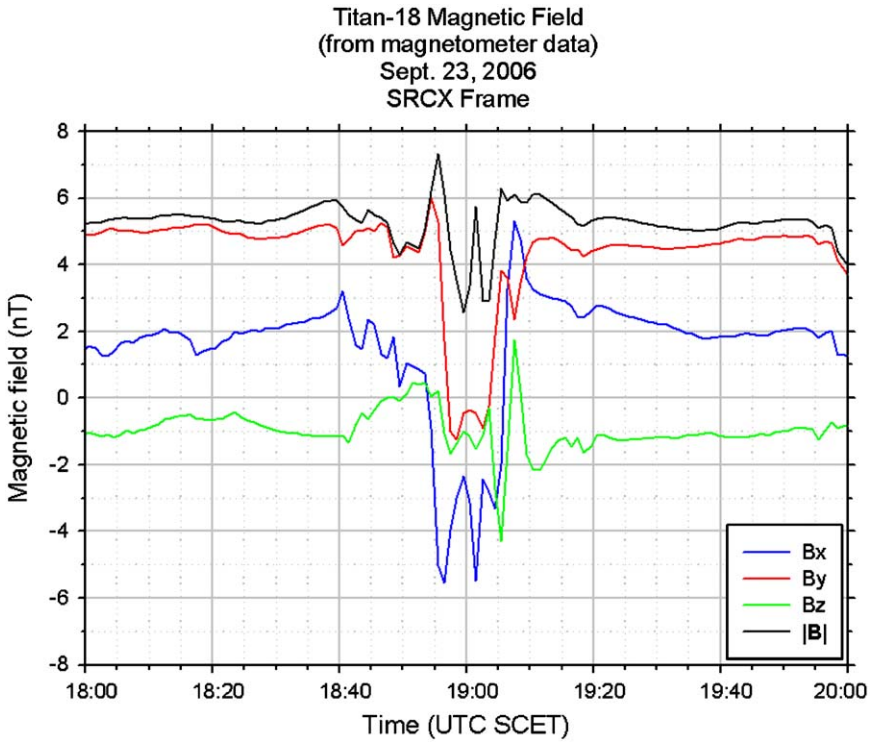

Fig. 12. Plot of magnetic field vector versus time for T18 encounter. Color key for each component shown on right.

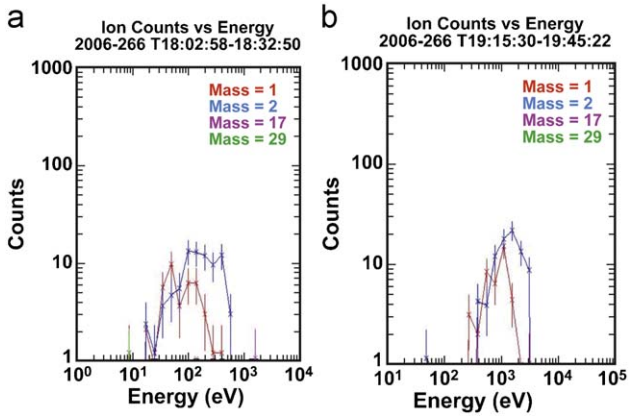

Fig. 13. Composition plot of ion counts versus energy for different mass groups. Same approach as that used in Fig. 9 for T9. Panel (a) is during the approach phase for the T18 encounter. The spacecraft is downstream for the flow past Titan. This panel shows the composition dominated by H^+ and H_2^+ with H_2^+ being more important than H^+. In panel (b) we have the brief event after closest approach and the flow has fully recovered and more upstream. Like in panel (a), the composition is dominated by H^+ and H_2^+ with H_2^+ having the higher counts. This figure shows the ion flux peaking near 1 keV/e, while for panel (a) the flux peaked around 200 eV/e.

corotation direction, the rotating flow will not be orthogonal to **B**. If one is observing pickup ions they are expected to move orthogonal to **B** and thus at right angles to the solar direction with outward radial velocity as observed. The finite $B_X > 1$ indicates $V_Y < 0$ is required for the flow, **V** to be perpendicular to **B**. During the inbound pass the viewing favors seeing the rotating flow, while on the outbound trajectory, after 19:20 SCET, the viewing is poor for seeing the rotating flow. This explains the greater signals for the external flow during the inbound period. Fig. 16 shows 2D θ–φ plots of the ion counts collapsed in energy for the inbound external flow. During the approach the spacecraft is somewhat downstream from Titan on the shadow side. It is seen that $T_\perp/T_\parallel \sim 2 > 1$ indicating the are consistent with pickup ions from Titan's extended H and H_2 exosphere, which have experienced some pitch angle scattering (i.e., could be shell distribution). Furthermore, the large time, ~4 min, separating peaks in ion count rate gives further evidence these ions are confined to a plane as expected for ring distributions. Consistent with this the ion beams are narrow in energy.

If the low-density plasma is predominantly freshly born pickup ions in the form of ring-like distributions, then the ion densities estimated using our ion moments program, which assumes $f(\boldsymbol{v})$ is broad compared to instrument's response $R(E,\theta,\varphi,\boldsymbol{v})$ are too high. A ring distribution is essentially a delta function in velocity space and thus $f(\boldsymbol{v})$ is narrow relative to the instrument's response (i.e., since so confined in velocity space they can yield high relative flux for low ion density). Referring to Fig. 14 for upstream region, the flux is closely confined in E/Q, very narrow in actuator angle (i.e., large time between observed ion beams) and confined to a narrow range of angular sectors are all consistent with narrow ion beams in velocity space. To correct for this narrowness in $f(\boldsymbol{v})$, one can use the expression in Sittler et al. (2004) for the instrument's count rate for a ring distribution, and equate this count rate, CR, to that for the Maxwellian. The GF drops out giving

$$N_b = (2\pi/\Delta\varphi)(\Delta\Omega\Delta E/E)/(2\pi)^{3/2}(V_b/w_{obs})^3 N_{obs}$$

In this expression N_b is the ion density for ring distribution, $\Delta\varphi \sim 20^\circ$ is the angular sector width of the instrument or azimuth, $\Delta\Omega = \sin\theta\, d\theta d\varphi$ is the angular width of the instrument's response in steradians with $d\theta \sim 8^\circ$, $\Delta E/E \sim 16\%$ is the energy width of the instrument, $V_b \sim 84$ km/s is the observed flow speed of the plasma, $w_{obs} \sim 60$ km/s is the observed thermal width of the ions and N_{obs} is the observed density. N_{obs}, w_{obs} and V_b are estimated by ion moments. For protons $V_b/w_{obs} \sim 1.4$ and $N_{obs} \sim 0.014$ ions/cm^3 for protons at 1816:18 so $N_b(H+) \sim 0.01 \times (1.4)^3 \times N_{obs} \sim 0.03 \times N_{obs} \sim$

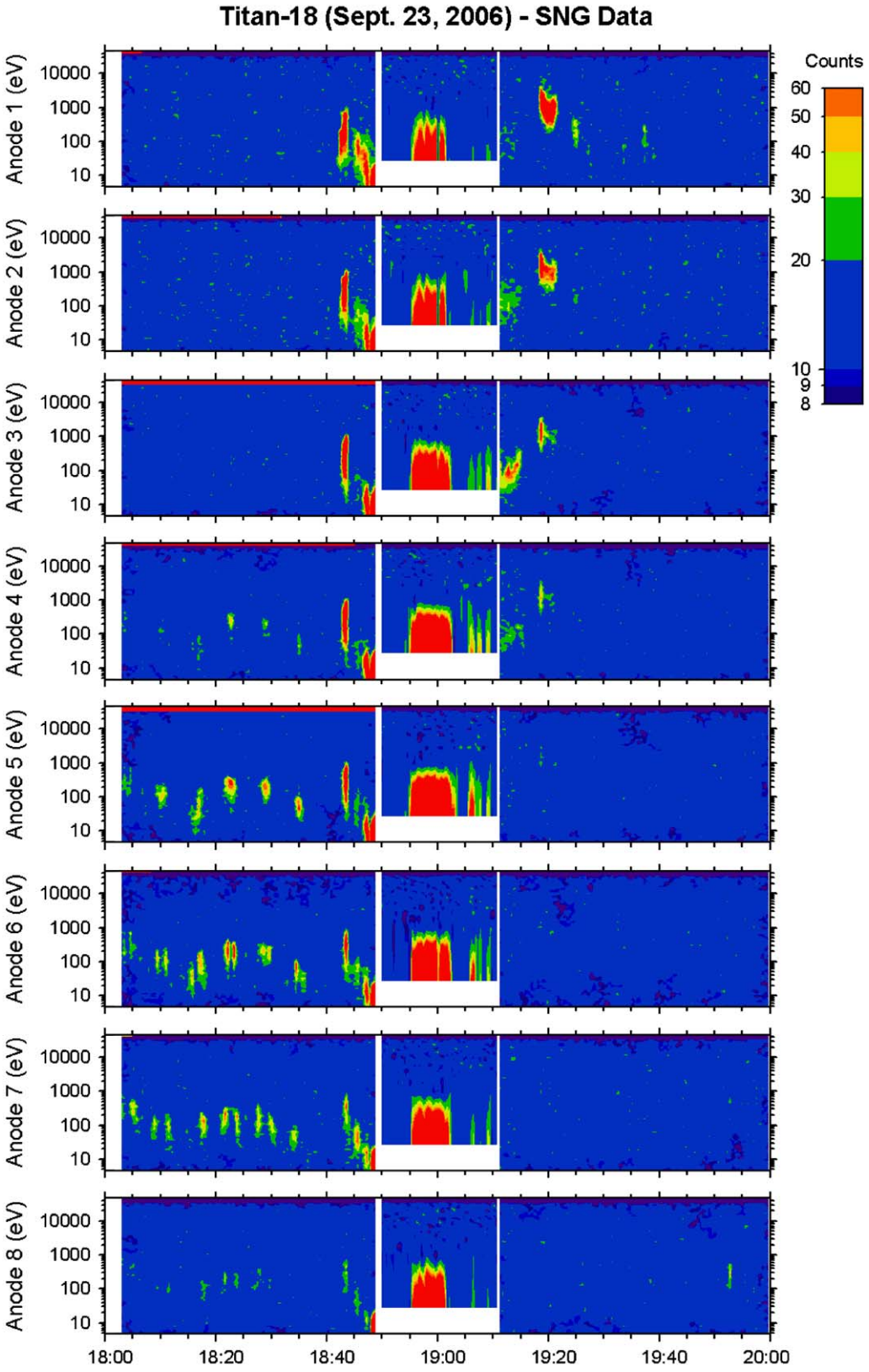

Fig. 14. Energy-time spectrogram plot for IMS ion singles for the T18 encounter. There are eight panels for each of the instrument's eight angular sectors or anodes. Centered about closest approach the instrument uses a different energy sweep table so that the min energy measured is 28 eV/e. This is to prevent the IMS microchannel plates (MCP) counting to levels faster than they are designed to handle when in the ionosphere and very high counting rates are expected. Before closest approach we do see evidence of upstream ions, while after 19:20 SCET the signal is undetectable due to poor viewing of the rotating flow. This low signal extends for several hours after 20:00 SCET.

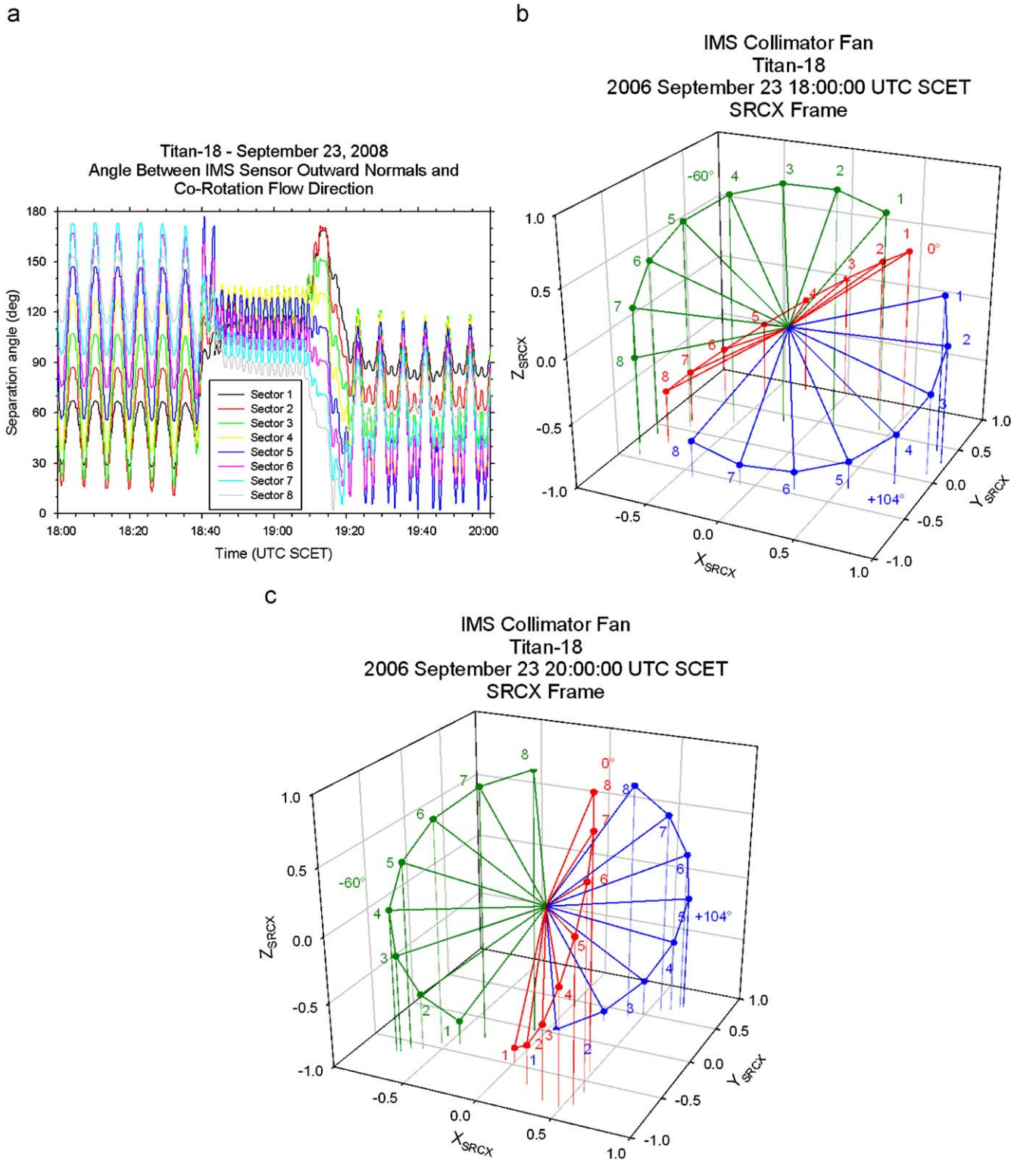

Fig. 15. Panel A shows the IMS field of view (FOV) for T18 relative to the corotation direction for each of the eight angular sectors. When the angle is at 180° the flow is directly into the instruments angular sector or anode of interest. The up-down motion to the curves is due to the actuator motion of the instrument. Panel B shows fan plot before closest approach and external flow around Titan. Panel C shows fan plot after closest approach when viewing of rotating flow was poor. In Fig. 14 one sees the ion beam at 18:20 SCET is centered on anodes 5 and 6. Angular sectors 6 and 7 are most favored for corotating flow, which indicates a slight deflection from corotation. For the outbound flow near Titan anodes 1 and 2 have the peak flux. The figure shows we may have just caught a brief period of good viewing. For the rest of the outbound period the viewing is not optimal for detecting the rotating flow of the magnetosphere and may explain the low fluxes outbound.

4.14×10^{-4} ions/cm^3. For H_2^+ one has $V_b/w_{obs}\sim1.2$ and $N_{obs}\sim0.017$ ions/cm^3 so $N_b(H_2^+)\sim3.25\times10^{-4}$ ions/cm^3. These give a total ion density of $\sim7.4\times10^{-4}$ ions/cm^3. From 18:16 to 18:26 the electron density $N_e\sim3.0\times10^{-3}$ el/cm^3 (see Fig. 17), which is a factor of 4 greater than the estimate using a ring distribution but a factor of 10 less than the ion moment estimate. Since the ring distribution estimate is a factor of 4 lower than the electron density, this calculation indicates some scattering is present and $f(\boldsymbol{v})$ is not the

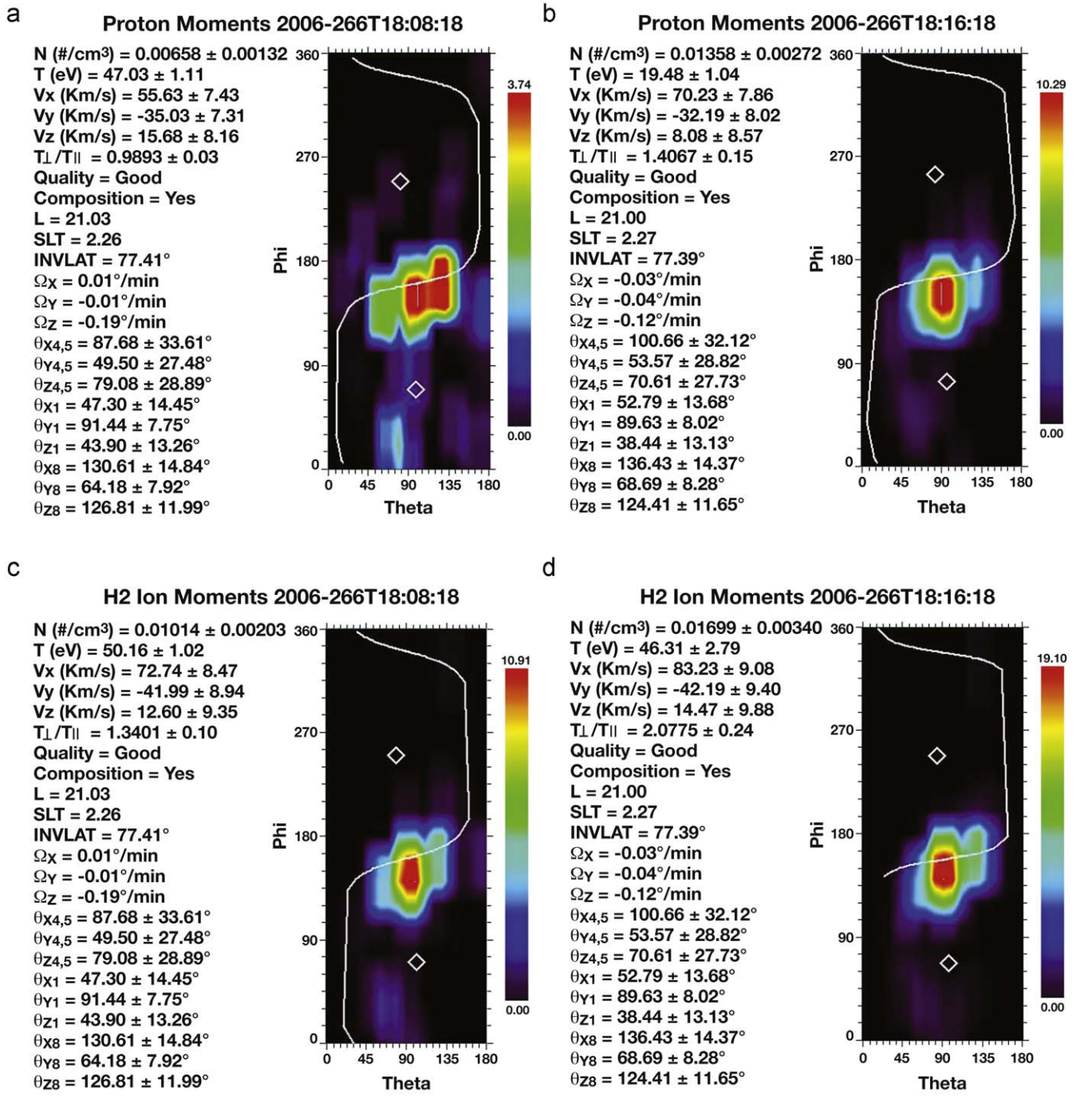

Fig. 16. 2D θ, φ plots of energy integrated ion counts for upstream ions before closest approach. Panel a is for protons at 18:08:18 and panel b is for protons at 18:16:18. Panels c and d are for mass 2 ions (H_2^+) for same time as panels a and b, respectively.

extreme case of a delta function in velocity space (i.e., presence of scattering supported by the observed modest temperature anisotropies $1 < T_\perp/T_\parallel < 2$). The charge neutrality condition, used here, is just one piece of evidence, which tends to exclude bi-Maxwellians for the ion distribution function.

The low densities of the magnetospheric plasma $n_e < 0.005$ el/cm^3, are consistent with Titan being at high magnetic latitudes and similar to what we often refer to as lobe field lines. The magnetic field $B \sim 7$ nT is higher than is typical, $B \sim 5$ nT, when the field is dipolar. This is further evidence for lobe-like field lines (i.e., Harris current sheet, see Arridge et al., 2007). In Fig. 17 is shown the ELS electron plasma data in a format similar to that for the ion singles data. This data indicates that there is a large flux of spacecraft emitted photoelectrons up to 20 eV and a low flux of magnetospheric electron ~ 100 eV. Since our ion analysis does not include spacecraft charging effects, and proton energies are ~ 50–100 eV inbound, one will tend to underestimate the proton flow speeds (see Sittler et al., 2006, 2007). Outbound proton energies are ~ 1 keV so spacecraft charging corrections are small. At sometimes there is no observable signal. Like T9 the plasma $\beta \ll 1$. Since H_2^+ fluxes are also significant for the external flow, they are likely produced by photoionization of Titan's H_2 exosphere. Therefore, the low observed magnetospheric electron fluxes are consistent with H_2^+ greater than protons by number for

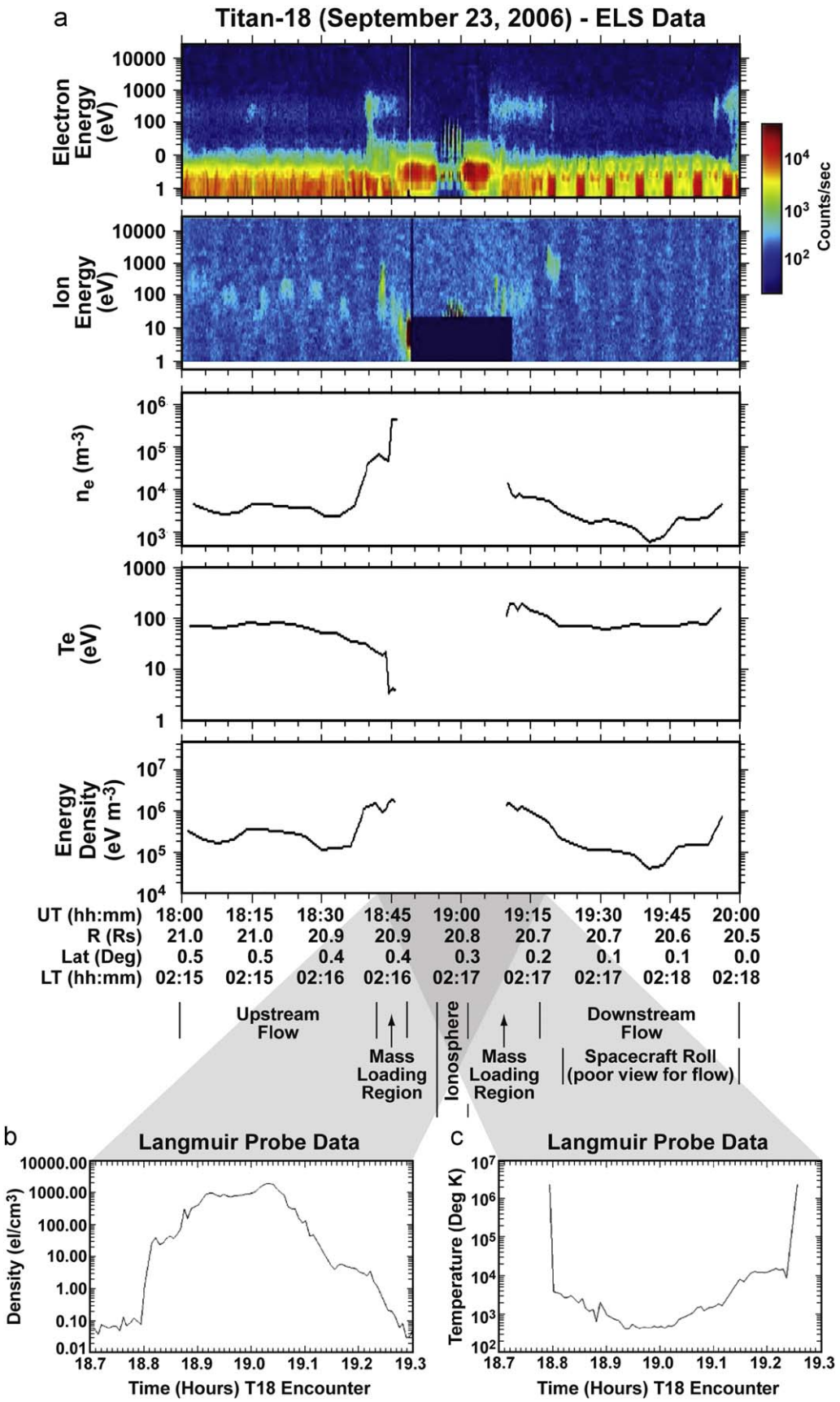

Fig. 17. Panel a shows energy-time spectrogram plot for ELS electron counts for the T18 encounter. Same format as shown Fig. 5 for T9 is used. Next sub-panel down shows energy–time spectrogram for IMS single data, next three sub-panel down show electron density, electron temperature and electron energy density, respectively. In panel b is shown ionospheric electron densities measured by the Langmuir Probe (LP) and in panel c is ionospheric electron temperature also measured by the LP. For electrons, top panel, below 10 eV the signal is dominated by photelectrons emitted by the spacecraft and spacecraft potentials >10 V must be present. Between 1847 and 1907 the spacecraft is within Titan's ionosphere and the electron fluxes are Titan ionosphere photoelectrons and not spacecraft emitted photoelectrons. Here one expects the spacecraft to be negatively charged. The gray shading shows the LP measurements in panels b and c occur when spacecraft is within ionosphere. Within the ionosphere the plasma beta $\beta \sim 10$ is very high as expected.

the external flow. In order to test this hypothesis in a more quantitative fashion, one can show the pickup ion density to be $N_{H_2^+} \sim N_0(H_2)R_0^2 K\pi/(bV)$ where $N_0(H_2) \sim 6.4 \times 10^4$ mol/cm^3 is the H_2 density at a reference height or radius $R_0 \sim 10{,}000$ km. In addition, $K \sim 7.6 \times 10^{-10}$ s^{-1} (photoionization plus charge exchange from Sittler et al., 2005), b=impact parameter $\sim$10,000 km and V=external flow speed $\sim$100 km/s one estimates an H_2^+ density $N_{H_2^+} \sim 0.004$ ions/cm^3, which is close to the observed electron density ~ 0.003 el/cm^3 (i.e., total $H^+ + H_2^+$ ion density) within experimental errors. Here, we have assumed a $1/r^2$ dependence for the H_2 exosphere. Considering the uncertainties the observations favor the interpretation that we are observing locally produced pickup ions from Titan's extended H_2 exosphere.

The typical Saturn magnetosphere plasma interaction with Titan, when the plasma is composed primarily of H^+, H_2^+ and W^+ ions as is the case during the Voyager 1 and TA flybys, has been simulated by a number of investigators and is reasonably understood. The cases described here for the T9 and T18 flybys are considerably different because they occur well away from the current sheet so that only light ions, such as protons and molecular hydrogen ions, in the upstream magnetosphere plasma are incident onto Titan's exosphere. Since the ambient ion density is so low H^+, H_2^+ pickup ions born from Titan's extended H and H_2 exosphere dominate by number the local plasma. This new environment has recently been described in the hybrid simulations of Lipatov et al. (2009). In this case, primarily Titan's own pickup ions interact with its neutral atmosphere and ionosphere to form a cavity with many similarities to those found during the V1 and TA flybys, where the background plasma was primarily magnetospheric. In all cases, the light ions H^+, H_2^+, play the major role in the formation of the plasma cavity encompassing the induced magnetosphere. The main difference is that the light ions for V1 and TA are magnetospheric while those for T9 and T18 are predominantly Titan's pickup ions. The hybrid model (Lipatov et al.,2009) shows that when the upstream flow is dominated by light ions, Titan's induced magnetosphere becomes inflated and its outer boundary or magnetopause moves outward. As the topside ionosphere expands well above the neutral exobase, it eventually rises above the collision dominated ionosphere, reaching the ion exobase. Above this altitude, the plasma is collisionless and less gravitationally bound than the ionosphere below. The simulations also show that one may expect to see heavy pickup ions during Event 2 for T9 but at a reduced level relative to the lighter pickup ions.

If one uses the boundary defined by the mass loaded ion data (H^+ and H_2^+ ion composition for this boundary crossing) this boundary forms near 1847 SCET relative to closest approach $\sim$1858 SCET at 950 km altitude. This boundary is at $r \sim 5300$ km and if the exobase at $r \sim 4000$ km (Sittler et al., 2005) is assumed to be correct, then this boundary is $\sim$1300 km above the exobase. Referring to the exosphere model by Sittler et al. (2005) shown in Fig. 18, the N_2 neutral density is negligible at this boundary and CH_4 is nearly 3 orders of magnitude below its exobase level. Furthermore, since the $\mathbf{E} = -\mathbf{V} \times \mathbf{B}$, the electric field points in the $-Z$ direction, one may not expect to see heavy pickup ions as observed for T_A (Hartle et al., 2006a, b) and Voyager 1 (Hartle et al., 1982 and Sittler et al., 2005). In the case of TA Hartle et al. (2006a,b) observed pickup ion beams of CH_4^+ and N_2^+ coming from Titan consistent with penetration of the flow down near Titan's exobase. These ion beams are expected when the ion gyro-radius $\sim$5000 km is much greater than the atmospheric scale height $\sim$100 km (see Hartle and Sittler, 2007). The large ion gyro-radii will occur if the rotational electric field can penetrate down to exobase heights. Note, the hybrid simulations by Lipatov et al. (2009) do show some penetration of the flow and some pickup methane ions may be observable (i.e., refer to weak detection of mass 16 ions for T9 Event 2). Heavy ionospheric ions are only observed near closest approach 1858 SCET when the spacecraft enters Titan's ionosphere. During the approach phase the spacecraft is somewhat downstream from Titan, which may also account for the higher altitude of this boundary. Fig. 17 also shows the presence of heavy negative ions for angular sectors 4 and 5 within Titan's ionosphere as originally reported by Coates et al. (2007a, b). Since, T18 is a polar pass (Fig. 2), the spacecraft

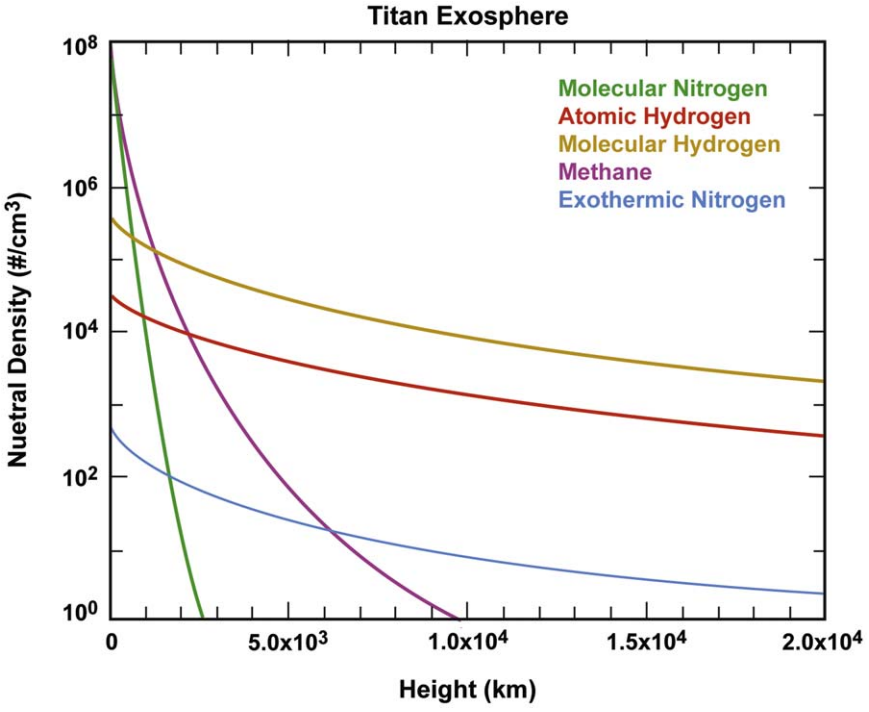

Fig. 18. Exosphere model for Titan from Sittler et al. (2005). The exosphere model includes N_2, CH_4, N*, H_2 and H neutrals. Neutrals are identified by their color code.

is always in sunlight and the ionosphere should be well developed along the spacecraft track. The spacecraft also moves nearly parallel to the terminator and like T9 the flow impinges onto Titan's nightside atmosphere. The ion singles data in Fig. 14 shows an outbound outer boundary ~1907 SCET with $r\sim4475$ km and only 475 km above-modeled exobase $r\sim4000$ km (H^+ and H_2^+ ions dominate the composition on the side outside this boundary), while hot ~200 eV electrons in Fig. 17 show a similar boundary at ~1907 SCET. This penetration of hot electrons to lower altitudes could be due to the flow being incident upon the nightside atmosphere where the convective electric field will not be short circuited by Titan's conductive ionosphere. The spacecraft is also more on the upstream side where the nightside ionosphere is less able to deflect the flow. The stronger lobe-like field will also drag the external flow to lower altitudes. With regard to the unshielded convective electric field, one may expect to see N_2^+ and CH_4^+ pickup ions from their neutral exospheres if looking upward since convective electric field is expected to point downward into Titan's ionosphere. Referring to Fig. 15c the CAPS IMS FOV does look upward and away from Saturn during its actuator scans. So, one might expect to see the heavy pickup ions, but are not observed. The fields are draped and changing in a complex way which may steer them outside the instrument's FOV. The magnetic field signatures show evidence of a boundary at ~1842 SCET inbound similar to that for the ion singles data, while one sees evidence of a current layer at ~1907 SCET, which is consistent with both the ion and electron data. The flip in polarity of both B_Y and B_X is consistent with draped field lines.

Although reserved for a later paper, the H_2 corona could have a large influence far from Titan. The plasma beta is much less than 1 and the flow energy density is also much less than the magnetic field energy density. This might also contribute to the very low electron fluxes within Titan's Hill sphere which is ~51,500 km or ~2.4 h before closest approach. The same may be also true for T9, but since the upstream flow is more detectable and dominated by H^+ relative to H_2^+, electron fluxes are higher as observed (i.e., electron impact ionization tends to dissociate the H_2 and produce primarily H^+). T9 is also probably closer to the current sheet than T18. In summary, the T18 flyby has a very similar interaction with Saturn's magnetosphere to that of T9 and represents a low energy limit of the magnetosphere interaction with Titan. In contrast to this, T5, represents a high energy limit for magnetospheric input to Titan's upper atmosphere (see Ågren et al., 2007; Hartle et al., 2006c, d), while TA represents a more intermediate case (Hartle et al., 2006a, b). One might expect the induced magnetopause for T18 to be further out than observed due to the lower plasma pressure, but the magnetic field pressure is twice that for dipolar field conditions which may then move the boundary to lower altitudes (i.e., pointing flux $\mathbf{S}=\mathbf{V}(B^2/4\pi)$).

6. Conclusion

We have presented new results for the T9 and T18 flybys for which the upstream plasma is predominantly composed of light ions, H^+ and H_2^+ and, since Titan is at SLT~0300 h Saturn's magnetosphere is locally in a magnetodisk configuration (Arridge et al., 2007 and Bertucci et al., 2009), with Titan below the magnetospheric current sheet. This paper offers the first full description of the fluid parameters for a Titan–Saturn-magnetosphere interaction that differs considerably from the interaction typically simulated following the Voyager flybys of Titan. Because Titan moves in and out of the plasma sheet as it orbits, such fluid parameters are needed to describe the orbit averaged atmospheric loss rate and the rate and composition of the supply of plasma to Saturn's outer magnetosphere. With a thin current sheet ~2° thick, see later discussions, Titan is more likely to be in lobe-like field lines than within the magnetospheric current sheet. The results presented here include fluid parameters for the ions and a revision of electron fluid parameters presented in Coates et al. (2007a). These parameters are compared to results from recent simulations (Modolo et al., 2007b; Lipatov et al., 2009). Preliminary results for the ions were presented by Szego et al. (2007).

The fluid parameters show predominantly azimuthal upstream ion flows in excess of corotation, $V_X\sim250$ km/s, for T9 inbound, while T9 outbound flow is less than corotation, $V_X\sim110$ km/s. For T18 inbound the external flow is sub-corotating with $V_X\sim84$ km/s (i.e., corotation speed ~200 km/s). Note, if one corrects for spacecraft potentials $\Phi_{SC}\sim+20$ V, the ion flow speeds could be as high as 100 km/s, but still sub-corotational. The magnetospheric ion densities are very low (2×10^{-3} ions/cm$^3 < N_{ION} < 0.1$ ions/cm^3) with magnetospheric proton temperatures ranging between 20 eV $< T_P <$ 200 eV and magnetospheric electron temperatures ranging between 50 eV $< T_e <$ 200 eV. For T18 inbound H_2^+ upstream ions have temperatures $T_{H_2}\sim50$ eV. The upstream flow also drifts perpendicular to **B**, with $T_\perp/T_\parallel > 1$. By using the electron density as a constraint, we were able to show that for T18 the upstream light ions are probably pickup ions from Titan's extended H and H_2 corona or exosphere. In both cases $B_X > 0$, but is small, so if flow is moving perpendicular to **B** then $V_Y < 0$ must hold, which is in fact observed. Sittler et al. (2009b) also showed that whenever close Titan encounters do not occur, but the spacecraft crosses near Titan's orbital radius, the ion densities tended to be near background levels and the plasma electrons are even at the detection limit for electron measurements, which are more sensitive than ion measurements. The Titan corona is expected to extend to about its Hill sphere, which is $\sim20R_T\sim51{,}500$ km. The escaping H and H_2 form a large torus around Saturn, with evidently lower H and H_2 neutral densities than that near Titan. Here we note, that Shemansky and Hall (1992) using Voyager ultraviolet observations showed an irregular distribution of atomic hydrogen with dominant source being Saturn's sunlit atmosphere but significant source in anti-solar direction at 20 Rs probably due to Titan. The above picture of the interaction region is supported by the hybrid model simulations of the T9 interaction by Lipatov et al. (2009). Their results show that, whenever Titan is within lobe-like magnetodisk field lines, it produces its own upstream plasma (otherwise plasma densities below detection levels) for subsequent interactions locally with Titan's heavy CH_4 and N_2 exosphere.

Using the ion and electron upstream parameters the plasma beta is low, $\beta \ll 1$, and the flow energy density $1/2\rho V^2\sim1.1\times10^{-11}$ erg/cm^3 is also small compared to the magnetic field energy density $B^2/8\pi\sim1.4\times10^{-10}$ erg/cm^3. Therefore the T9 and T18 flybys are low beta plasma interactions, while V1 observed a very high beta plasma interaction, $\beta\sim11$ (Neubauer et al., 1984). In the case of TA Cassini observed an intermediate plasma beta interaction $\beta\sim1$ (see Sittler et al., 2009a). The low β case described here is somewhat offset by the higher magnetic field strength with pressure $P_B\sim2$ times that for dipolar field conditions. Therefore, T9 and T18 represent the low energy limit of Saturn's magnetosphere input to Titan's upper atmosphere and ionosphere.

During T9 inbound, the upstream flow showed evidence of Alfvenic fluctuations with amplitude $\delta V_X\sim50$ km/s and magnetic field perturbation $\delta B_X\sim-1$ nT consistent with waves propagating along magnetic field lines. The cause of these Alfven-like waves is not yet known. But, comparison of δV_X and δB_X indicates the waves are not purely Alfvenic or there is an undetected heavy ion component in the plasma.

As shown in Sittler et al. (2009a, b) the proton only composition is a direct result of the magnetodisk geometry of Saturn's

magnetosphere at local times ~0300 LT (i.e., more likely to be in lobe-like field lines). This magnetospheric configuration may also apply for other local times within the midnight hemisphere of Saturn's magnetosphere. At these local times the solar wind does not confine the flow and the outwardly diffusing and rotating heavy ion plasma from the inner magnetosphere will tend to stretch out the magnetosphere into a magnetodisk geometry (Arridge et al., 2007). In Sittler et al. (2009b) it is shown that when the spacecraft is below or above rather than in the current sheet the composition changes from heavy ions with mass ~17 to light ions such as H^+ and H_2^+ and the ion number densities are very low. Maurice et al. (1997) showed that Jupiter's outer magnetosphere will form into a magnetodisk geometry so that protons dominate beyond a few degrees above or below the current sheet. Some hybrid models of the T9 encounter, such as Modolo et al. (2007b), argued that the upstream ion composition was probably dominated by heavy ions like Voyager 1, assuming that the plasma is highly time dependent. But, this is not the case for T9 or T18. Instead one expects the ion composition to be dominated by light ions when in magnetodisk configuration (i.e., T5 is exception to this).

During T9 Event 1 Cassini also observed topside ionospheric ions, mass 17 (CH_5^+) and mass 29 ($C_2H_5^+$), ions moving away from Titan down its induced magnetotail with ion number flux $\sim 7\times10^6$ ions/cm^2/s, with total density ~8 ions/cm^3, flow speeds ~7–9 km/s and ion temperatures ~3.4 eV (mass 17) and 4.9 eV (mass 29). This outflow can be compared with the Hartle et al. (2008a, b) calculations for TA. They inferred an outward ionospheric flux $\sim 10^7$ ions/cm^2/s with outward flow speed ~1 km/s at the topside ionosphere. Their estimate was made by employing the same procedure used by Hartle and Grebowsky (1995) for Venus. Using ionospheric measurements made from the Pioneer Venus Orbiter (PVO) they showed that upward flow and acceleration of H^+, D^+ and O^+ in the nightside ionosphere of Venus was produced by a strong polarization electric field. The same situation applies at Titan, when the ionosphere is a high beta plasma. Just below the exobase, the TA plasma and LP data reveal an ionospheric electron temperature $T_e\sim1000$ K that is considerably hotter than the ionospheric ions $T_{ION}<200$ K. In this situation, the electrons tend to drag the ions out. Thus, using the T18 LP data in Fig. 17 and spacecraft altitude in Fig. 3 and following the approach of Hartle et al. (2008a, b), one finds a strong upward polarization electric field force in the ionosphere that exceeds the gravitational force on an 1 amu ion, H^+, by more than 25 times. This is consistent with the CAPS measurements described here that yield an outward flux of heavy ions $\sim 7\times10^6$ ions/cm^2/s with speed ~7–9 km/s during Event 1 for T9. The number flux for mass 28 ions is similar to that estimated by Hartle et al. (2008a, b) for TA even though it was a high beta plasma encounter. In this case, magnetic forces are ignored, and the dominant net upward accelerating force is the sum of the upward polarization electric field force and the downward forces of gravity and ion drag. For Event 2 we observed an outward flux $\sim 10^6$ ions/cm^2/s with speed $\sim 63\pm10$ km/s, total ion density ~0.2 ions/cm^3, ion temperature $T_{ION}\sim12$–15 eV and ion composition dominated by the lighter ions H^+ and H_2^+. In both Events 1 and 2 the flow was away from Titan and about 30° from field aligned. Event 2 is interpreted as scavenged ions from Titan's corona at the induced magnetopause boundary. During Event 2 a previously undetected mass 16 ion (i.e., cannot exclude mass 17 ion) component was detected, which was probably methane pickup ions with energies ~50 eV or flow speeds ~25 km/s less than that observed by the light ions ~60 km/s. This plasma could be ionospheric but mass 29 was not detected, possibly because it was below the CAPS IMS detection threshold. There was also not enough signal to determine fluid parameter for the mass 16 ions.

In between Events 1 and 2 a very energetic $V_X\sim300$ km/s field aligned flow of protons was observed. The proton densities were ~0.015 protons/cm^3 and proton temperature $T_P\sim267$ eV or thermal speed $w_P\sim225$ km/s resulting in a sonic Mach number $M_S\sim1.5$. The temperature anisotropy was $T_\perp/T_\parallel\sim2.0$ indicating perpendicular heating. The plasma beta is low $\beta\sim0.23\ll1$, so that the magnetic field channels the flow. During this time $V_X\sim288$ km/s, $V_Y\sim+85$ km/s and $V_Z\sim-77$ km/s, while the magnetic field is $B_X\sim5$ nT, $B_Y\sim2$ nT and $B_Z\sim-1$ nT. This implied that the field is highly twisted along the x-direction consistent with draped field lines in the induced magnetotail. The understanding of the details will have to be deferred to later studies involving hybrid simulations of the interaction.

Unlike the distant T9 encounter across Titan's induced magnetotail, the T18 encounter approached close to 950 km altitude but exhibited similar external plasma conditions and SLT~0300 h. Like T9 Saturn's magnetosphere near Titan was in a magnetodisk configuration and Titan was below the current sheet on lobe-like field lines. The plasma density was very low with ion and electron densities $\sim3\times10^{-3}$ ions/cm^3, the ion upstream composition was dominated by light ions, H^+ and H_2^+, ion temperatures ~19 eV for protons and ~50 eV for H_2^+ ions and electron temperatures ~100 eV. The plasma beta $\beta\ll1$ with flow speeds ~84 km/s and drifting perpendicular to the magnetic field. It was shown that the upstream ions were probably pickup ions from Titan's H and H_2 exosphere as discussed above so that the interaction was also a low energy input interaction with Titan's atmosphere. The dominance of H_2^+ ions is consistent with the very low electron densities observed, which indicates photoionization and charge exchange dominate over electron impact ionization.

In conclusion, it has been shown that the T9 and T18 encounters occurred during periods when Saturn's magnetosphere was in a magnetodisk configuration, Titan was below the current sheet, upstream plasma densities were low and the upstream flow was dominated by the light ions protons and H_2^+. Bertucci et al. (2009) have shown that during local times centered on midnight a magnetodisk configuration at Titan's radial distances from Saturn is expected, while near noon local time a more dipolar configuration is expected. As T5 observations have shown, current sheet crossings for magnetodisk configurations can be dominated by keV heavy ions (Hartle et al., 2006c, d; Cravens et al., 2008) and very high energy interactions can occur. Since the current sheet is probably only a few degrees thick (see Maurice et al., 1997) they are less likely to occur while near noon local time interactions with heavy keV magnetospheric ions are expected to be more common (i.e., current sheet thicker), but may be intermediate to high energy interactions when compared to the interaction described here. It was also shown, in this paper that pickup ions from Titan's extended H and H_2 corona tended to dominate by number the upstream plasma for T9 and T18 and interactions ~Hill sphere dimensions relative to Titan center, 51,000 km, were observed. In the case of T9 and T18 upstream light ions dominate over heavy ions, so multi-fluid simulations may be applicable, since the ion gyro-radii are small. In contrast to T9 and T18 the Voyager 1 and Cassini T5 encounters are high energy interactions with heavy ions dominating the external flow, with TA being a more intermediate case. Therefore, for V1, T5 and TA hybrid simulations are required (see Ma et al., 2006). These differences in Titan's interaction with Saturn's magnetosphere may have a relationship with the observed correlation of Saturn Kilometric Radiation (SKR) emissions with Titan being near midnight local time (Menietti et al., 2007) where the magnetic field is expected to be in a magnetodisk configuration with Titan in lobe-like field lines and light ions dominate the external flow. This will be the subject of future investigations. After the early confusion about the nature of the interaction of the

magnetosphere with Titan's atmosphere, it is now exciting that the considerable variability and complexity in the nature of this interaction is becoming understood. Here we have contributed to that understanding by obtaining useful fluid parameters for the low energy type interaction.

Acknowledgements

This work was supported at NASA Goddard Space Flight center in part by the Cassini Plasma Spectrometer (CAPS) Project through NASA Jet Propulsion Laboratory contract 1243218 with the Southwest Research Institute in San Antonio, Texas. Additional support was provided at Goddard by the NASA Cassini Data Analysis Program (CDAP). We would also like to acknowledge the data analysis support by S. Bakshi from ADNET Systems Incorporate and R. Kilgore for graphic arts support from TRAX Corporation.

References

Ågren, K., Wahland, J.-E., Modolo, R., Lummerzheim, D., Galand, M., Muller-Wodard, I., Canu, P., Kurth, W.S., Cravens, T.E., Yelle, R.V., Waite Jr., J.H., Coates, A.J., Lewis, G.R., Young, D.T., Bertucci, C., Dougherty, M.K., 2007. On magnetospheric electron impact ionization and dynamics in Titan's ram-side and polar ionosphere, a Cassini case study. Ann. Geophys. 25, 2359–2369.

Arridge, C.S., Russell, C.T., Khurana, K.K., Achilleos, N., André, N., Rymer, A.M., Dougherty, M.K., Coates, A.J., 2007. Mass of Saturn's magnetodisc: Cassini observations. Geophys. Res. Lett. 34, L09108, doi:10.1029/2006GL028921.

Arridge, C.S., Russell, C.T., Khurana, K.K., Achilleos, N., Cowley, S.W.H., Dougherty, M.K., Southwood, D.J., Bunce, E.J., 2008a. Saturn's magnetodisc current sheet. J. Geophys. Res 113, A04214, doi:10.1029/2007JA012540.

Arridge, C.S., Khurana, K.K., Russell, C.T., Southwood, D.J., Achilleos, N., Dougherty, M.K., Coates, A.J., Leinweber, H.K., 2008b. Warping of Saturn's magnetospheric and magnetotail current sheets. J. Geophys. Res. 113, A08217, doi:10.1029/2007JA012963.

Arridge, C.S., Sittler, E.C., André, N., Coates, A.J., Dougherty, M.K., Fouad, G.-R., Gilbert, L.K., Khurana, K.K., Lewis, G.R., McAndrews, H.J., Russell, C.T., 2009, Plasma electrons in Saturn's magnetotail, JGR, doi:10.1016/j.pss.2009.02.009.

Backes, H., et al., 2005. Titan's magnetic field signature during the first Cassini encounter. Science 308, 992–995, doi:10.1126/science.1109763.

Bertucci, C., Neubauer, F.M., Szego, K., Wahlund, J.-E., Coates, A.J., Dougherty, M.K., Young, D.T., Kurth, W.S., 2007. Structure of Titan's mid-range magnetic tail: Cassini magnetometer observations during the T9 flyby, Geophys. Res. Lett. 34, L24S02, doi:10.1029/2007GL030865.

Bertucci, C., Sinclair, B., Achilleos, N., Hunt, P., Dougherty, M.K., Arridge, C.S., 2009. The variability of Titan's magnetic environment, Planet. Space Sci., doi:10.1016/j.pss.2009.02.009.

Coates, A.J., 2009. Interaction of Titan's ionosphere with Saturn's magnetosphere,. Philos. Trans. R. Soc. A: Math. Phys. Eng. Sci. 367 (1889), 773–788.

Coates, A.J., Crary, F.J., Young, D.T., Szego, K., Arridge, C.S., Bebsi, Z., Sittler Jr., E.C., Hartle, R.E., Hill, T.W., 2007a. Ionospheric electrons in Titan's tail: plasma structure during the Cassini T9 encounter. Geophys. Res. Lett. 34, L24S05, doi:10.1029/2007GL030919.

Coates, A.J., Crary, F.J., Lewis, G.R., Young, D.T., Waite Jr., J.H., Sittler Jr., E.C., 2007b. Discovery of heavy negative ions in Titan's ionosphere. Geophys. Res. Lett. 34, L22103, doi:10.1029/2007GL030978.

Cravens, T.E., Keller, C.N., Ray, B., 1997. Photochemical sources of non-thermal neutrals for the exosphere of Titan. Planet. Space Sci. 45 (8), 889–896.

Cravens, T.E., Vann, J., Clark, J., et al., 2004. The ionosphere of Titan: an updated theoretical model, 2004, Second World Space Congress/34th COSPAR Scientific Assembly, 10–19 October 2002 Houston, TX, Planet. Atmos. Ionos. Plasma Int. Adv. Space Res. 33, 212–215.

Cravens, T.E., Robertson, I.P., Clark, J., Wahlund, J.-E., Waite Jr., J.H., Ledvina, S.A., Niemann, H.B., Yelle, R.V., Kasprzak, W.T., Luhmann, J.G., McNutt, R.L., Ip, W.-H., De La Haye, V., Muller-Wodarg, I., Young, D.T., Coates, A.J., 2005. Titan's ionosphere: model comparison with Cassini Ta data. Geophys. Res. Lett. 32, L12108, doi:10.1029/2005GL023249.

Cravens, T.E., Robertson, I.P., Ledvina, S.A., Michell, D., Krimigis, S.M., Waite Jr, J.H., 2008. Energetic ion precipitation at Titan. Geophys. Res. Lett. 35, L03103.

Dobe, Z., Szego, K., Quest, K.B., Shapiro, Vtali D., Hartle, R.E., Sittler Jr., E.C., 2007. Nonlinear evolution of modified two-stream instability above ionosphere of Titan: comparison with the data of the Cassini plasma spectrometer. J. Geophys. Res. 112, A03203, doi:10.1029/2006JA011770.

Glassmeier, K.-H., 1980. Magnetometer array observations of giant pulsation event. J. Geophys 48, 127.

Gurnett, D.A., Scarf, F.L., Kurth, W.S., 1982. The structure of Titan's wake from plasma wave observations. J. Geophys. Res. 87, 1395–1403.

Hartle, R.E., Sittler Jr., E.C., Ogilvie, K.W., Scudder, J.D., Lazarus, A.J., Atreya, S.K., 1982. Titan's ion exosphere observed from Voyager 1. J. Geophys. Res. 87, 1383.

Hartle, R.E., Grebowsky, J.M., 1995. Planetary loss from light ion escape on Venus. Adv. Space Res. 15 (4), 117–122.

Hartle, R.E., Sittler Jr., E.C., Neubauer, F.M., Johnson, R.E., Smith, H.T., Crary, F., McComas, D.J., Young, D.T., Coates, A.J., Simpson, D., Bolton, S., Reisenfeld, D., Szego, K., Berthelier, J.J., Rymer, A., Vilppola, J., Steinberg, J.T., Andre, N., 2006a. Preliminary interpretation of titan plasma interaction as observed by the Cassini plasma spectrometer: comparisons with Voyager 1. Geophys. Res. Lett. 33, L08201, doi:10.1029/2005GL024817.

Hartle, R.E., Sittler Jr., E.C., Neubauer, F.M., Johnson, R.E., Smith, H.T., Crary, F., McComas, D.J., Young, D.T., Coates, A.J., Simpson, D., Bolton, S., Reisenfeld, D., Szego, K., Berthelier, J.J., Rymer, A., Vilppola, J., Steinberg, J.T., Andre, N., 2006b. Initial interpretation of titan plasma interaction as observed by the Cassini plasma spectrometer: comparisons with Voyager 1. Planet. Space Sci. 54, 1211.

Hartle, R., the Cassini Titan Team, 2006c. Saturn's magnetosphere plasma interaction with Titan's exosphere and ionosphere: structure and composition, Europlanet Meeting, Berlin, EPSC2006-A-00305.

Hartle, R.E., Sittler, E.C., Shappirio, M.D., Johnson, R.E., Luhmann, J.G., Ledvina, S.A., Cooper, J.F., Coates, A.J., Szego, K., Burger, M.H., Simpson, D.G., Crary, F., Young, D.T., 2006d. Saturn magnetosphere ion erosion by Titan: penetration and loss of water group ions in upper atmosphere. EOS Trans. AGU 87 (52).

Hartle, R.E., Sittler Jr., E.C., 2007. Pickup ion phase space distributions: effects of atmospheric spatial gradients. J. Geophys. Res 112, A07104, doi:10.1029/2006JA012157.

Hartle, R., Sittler E., Lipatov, A., 2008a. Ion escape from the ionosphere of Titan. Geophysical Research Abstracts, vol. 10, EGU2008-A-09860.

Hartle, R.E., Sittler Jr., E.C., Lipatov, A., 2008b. Comparison of ion escape from wake-side ionospheres of Venus and Titan. EOS Trans. AGU 89 (53).

Huebner, W.F., Giguere, P.T., 1980. A model of comet comae II. Effects of solar photodissociation ionization. Astrphys. J. 238, 753.

Johnson, R.E., Tucker, O.J., Michael, M., Sittler Jr., E.C., Smith, H.T., Young, D.T., Waite Jr., J.H., 2009. Mass loss processes in Titan's upper atmosphere. In: Brown, R.H., Lebreton, J.–P., Waite Jr., J.H. (Eds.), Titan from Cassini-Huygens. Springer.

Lipatov, A., Sittler Jr. E.C., Hartle, R.E., 2009. Titan's plasma environment for T9 encounter: 3D hybrid simulation and comparison with observations, 2009 EGU, TBD.

Ma, Y., Nagy, A.F., Cravens, T.E., Sokolov, I.V., Hansen, K.C., Wahlund, J.-E., Crary, F.J., Coates, A.J., Dougherty, M.K., 2006. Comparisons between MHD model calculations and observations of Cassini flybys of Titan. J. Geophys. Res. 111, A05207, doi:10.1029/2005JA011481.

Maurice, S., Blanc, M., Prange, R., Sittler Jr., E.C., 1997. The magnetic-field-aligned polarization electric field and its effects on particle distribution in the magnetospheres of Jupiter and Saturn. Planet. Space Sci. 45 (11), 1449–1465.

Menietti, J.D., Groene, J.B., Averkamp, T.F., Hospodarsky, G.B., Kurth, W.S., Gurnett, D.A., Zarka, P., 2007. Influence of Saturnian moons on Saturn kilometric radiation. J. Geophys. Res. 112, A08211, doi:10.1029/2007JA012331.

Modolo, R., Wahlund, J.-E., Bostrom, R., Canu, P., Kurth, W.S., Gurnett, D., Lewis, G.R., Coates, A.J., 2007a. Far plasma wake of Titan from the RPWS observations: a case study, Geophys. Res. Lett., 34, L24S04, doi:10.1029/2007GL030482.

Modolo, R., Chanteur, G.M., Wahlund, J.–E., Canu, P., Kurth, W.S., Gurnett, D., Matthews, A.P., Bertucci, C., 2007b. Plasma environment in the wake of Titan from hybrid simulation: a case study, Geophys. Res. Lett., 34, L24S07, doi:10.1029/2007GL030489.

Modolo, R., Chanteur, G.M., 2008. A global hybrid model for Titan's interaction with the kronian plasma: application to the Cassini Ta flyby. J. Geophys. Res. doi:10.1029/2007JA012453.

Neubauer, F.M., Gurnett, D.A., Scudder, J.D., Hartle, R.E., 1984. Titan's magnetospheric interaction. In: Gehrels, T., Matthews, M.S. (Eds.), Saturn. University of Arizona Press, Tucson, pp. 760–787.

Neubauer, F.M., et al., 2006. Titan's near magnetotail from magnetic field and electron plasma observations and modeling: Cassini flybys, TA, TB and T3. J. Geophys. Res. 111, A10220, doi:10.1029/2006JA011676.

Rapp, D., Englander-Golden, P., 1965. Total cross-sections for ionization and attachment in gases by electron impact I, Positive ionization. J. Chem. Phys. 43, 1464.

Shemansky, D.E., Hall, D.T., 1992. The distribution of atomic hydrogenin the magnetosphere of Saturn. J. Geophys. Res. 97, 4143.

Sillanpaa, I., Kallio, E., Janhunen, P., Schmidt, W., Mursula, J., Vilpolla, Tanskanen, P., 2006. Hybrid simulation study of ion escape at Titan for different orbital positions. Adv. Space Res. 38, 799–805.

Sittler Jr., E.C., Hartle, R.E., Vinas, A.F., Johnson, R.E., Smith, H.T., Mueller-Wodarg, I., 2004. Titan interaction with Saturn's magnetosphere: mass loading and ionopause location. In: Proceedings of the International Conference TITAN from Discovery to Encounter, ESA Spec. Publ. 1278, p. 377, ESTEC, Noordwijk, The Netherlands.

Sittler Jr., E.C., Hartle, R.E., Vinas, A.F., Johnson, R.E., Smith, H.T., Mueller-Wodarg, I., 2005. Titan interaction with Saturn's magnetosphere: Voyager 1 results revisited. J. Geophys. Res. 110, A09302, doi:10.1029/2004JA010759.

Sittler Jr., E.C., et al., 2006. Cassini observations of Saturn's inner plasmasphere: Saturn orbit insertion results. Planet. Space Sci. 54, 1197–1210.

Sittler Jr., E.C., Thomsen, M., Johnson, R.E., Hartle, R.E., Burger, M., Chornay, D., Shappirio, M.D., Simpson, D., Smith, H.T., Coates, A.J., Rymer, A.M., McComas, D.J., Young, D.T., Reisenfeld, D., Dougherty, M., Andre, N., 2007. Erratum to

"Cassini observations of Saturn's inner plasmasphere: Saturn orbit insertion results" [Planetary and Space Science 54 (2006) 1197–1210].

Sittler Jr., E.C., Hartle, R.E., Bertucci, C., Coates, A.J., Cravens, T.E., Dandouras, I., Shemansky, D., 2009a. Chapter 16: Energy deposition processes in Titan's upper atmosphere and its induced magnetosphere. In: Brown, R.H., et al. (Eds.), Titan from Cassini-Huygens. Springer.

Sittler Jr., E.C., Hartle, R.E., Lipatov, A.S., Cooper, J.F., Bertucci, C., Coates, A.J., Arridge, C., Szego, K., Johnson, R.E., Shappirio, M., Simpson, D.G., Tokar, R., Young, D.T., 2009b. Saturn's magnetosphere and properties of upstream flow at Titan: preliminary results, Planet. Space Sci., (submitted for publication).

Szego, K., Bebesi, Z., Bertucci, C., Coates, A.J., Crary, F., Erdos, G., Hartle, R., Sittler Jr. E.C., Young, D.T. 2007. Charged particle environment of titan during the T9 flyby, Geophys. Res. Lett., 34, L24S03, doi:10.1029/2007GL030677.

Vuitton, V., Yelle,, R.V., McEwan, M.J., 2007. Ion chemistry and N-containing molecules in Titan's upper atmosphere. Icarus 191, 722–742.

Wahlund, J.-E., Bostrom, R., Gustafsson, G., Gurnett, D.A., Kurth, W.S., Pedersen, A., Averkamp, T.F., Hospodarsky, G.B., Persoon, A.M., Canu, P., Neubauer, F.M., Dougherty, M.K., Eriksson, A.I., Morooka, M.W., Gill, R., Andre, M., Eliasson, L., Muller-Wodarg, I., 2005. Cassini measurements of cold plasma in the ionosphere of Titan. Science 308, 986–989.

Wei, H.Y., Russell, C.T., Wahlund, J.-E., Dougherty, M.K., Bertucci, C., Modolo, R., Ma, Y.J., Neubauer, F.M., 2007. Geophys. Res. Lett., 34, L24S06, doi:10.1029/2007GL030701.

Wilson, R.J., Tokar, R.L., Henderson, M.G., Hill, T.W., Thomsen, M.F., Pontius D.H., Jr., 2008. Cassini plasma spectrometer thermal ion measurements in Saturn's inner magnetosphere. J. Geophys. Res. 113, A12218, doi:10.1029/2008JA013486.

Young, D.T., et al., 2004. Cassini plasma spectrometer investigation. Space Sci. Rev. 114, 1–112.